

Genesis and role of bitumen in fracture development during early catagenesis

Israa S. Abu-Mahfouz^{1*}, Joe Cartwright¹, Erdem Idiz¹, John N. Hooker², Stuart Robinson¹, Sander van den Boorn³

¹ *University of Oxford, Department of Earth Sciences, South Parks Road, OX1 3AN Oxford, United Kingdom*

² *Pennsylvania State University, Department of Geosciences, 503 Deike Bldg., University Park, 11Pennsylvania, USA*

³ *Shell Projects and Technology, Grasweg 31, 1031 HW Amsterdam, The Netherlands*

*Corresponding author (e-mail: isra.abumahfouz@spc.ox.ac.uk)

ABSTRACT

Bitumen-bearing fractures and vugs were investigated in the highly organic-rich Jordan Oil Shale (JOS) of Late Cretaceous to Eocene age, which has potential as a highly fractured, unconventional hydrocarbon play. Bitumen is present as macroscopically visible deposits and as inclusions in the cement of abundant natural fractures and adjacent vugs. The frequency of bitumen occurrence in fractures closely correlates with Total Organic Carbon (TOC) and burial depth. Petrographic and organic-geochemical analyses on bitumen samples extracted from fractures and their host rock matrix show that the fracture-filling bitumen comprises indigenous low maturity hydrocarbons derived from the surrounding organic-rich Oil Shale and has not migrated from a deeper source. Maturity indicators imply that the oil shale is in the pre-oil generation stage of early catagenesis throughout the investigated area, but with a regional increase in thermal maturity from west to east as the result of greater maximum burial depth. Bitumen mobilization in the host rock was mainly controlled by vertical loading stress acting on the non-Newtonian bitumen phase in load bearing configurations in the organic-rich matrix. Bitumen fractures were developed by hydraulic fracturing as the result of fluid overpressure in the organic matter. Overpressured bitumen has acted as a fracture driver, generating bitumen veins in both the organic-rich mudstones and the adjacent chert and silicified intervals.

27 **Keywords:** Bitumen, Hydrocarbons, Biomarkers, Fractures, Jordan Oil Shale, Unconventional.

28 Natural fractures play an important role in hydrocarbon migration and accumulation (Nelson 1985;
29 Mandl & Harkness 1987; Jones *et al.* 1998; Aydin 2000; Childs *et al.* 2009; Wang *et al.* 2016).
30 Hydrocarbons in the form of solid bitumen have been documented within fractures and pores in
31 reservoirs and overlying seal rocks. These occurrences **are present** on a range of scales, including
32 bitumen in large-scale structures such as Gilsonite dikes (Verbeek & Grout 1983, 1992), in mineralized
33 veins (Parnell *et al.* 2003, 2017a, 2017b; Fink 2016) and in microfractures (Ryder *et al.* 2013).
34 Most of the studies have focused on investigating bitumen occurrences that are hosted in stratigraphic
35 units other than the source rock from which the bitumen was derived, and have used a variety of research
36 methodologies including experimental work, field-based investigations and conceptual modelling (e.g.,
37 Parnell *et al.* 1991, 1994; Peters *et al.* 1996; Parnell & Monson 1998; Wilhelms *et al.* 2001; Wang *et al.*
38 2015). There is, however, a paucity of studies that focus on solid bitumen formation and migration
39 within the confines of the source rock interval, and as a result, there are many unresolved questions
40 concerning this earliest phase of hydrocarbon mobilisation (Pepper 2017).
41 The prolific oil shale deposits of Late Cretaceous to Palaeogene age in Jordan provide an excellent
42 opportunity to study the earliest stages of catagenesis, and in particular the factors leading to the
43 formation of bitumen veins, and bitumen inclusions in mineralized veins. The oil shales are
44 characterised as one of the richest oil shales in the world (Jaber *et al.*, 1997; Hamarneh 1998; Dyni,
45 2006), and are widely developed in Jordan. They are identified both in outcrop and across a large area
46 in the subsurface through drilling operations in the past 20 years. The oil shales have been studied
47 previously for their organic matter enrichment, maturation, hydrocarbon potential and sedimentological
48 and palaeo-environmental implications (Abed *et al.* 2005; Abed & Arouri 1994; Abed *et al.* 2009; Ali
49 Hussein *et al.* 2014a, 2014b; Hakimi *et al.* 2016, 2018; März *et al.* 2016). The organic geochemical
50 characteristics of bitumen were only studied for bitumen present within the oil shale matrix (e.g., Abed

51 *et al.* 2005; Hakimi *et al.* 2016). Fracture-filling bitumen present in these rocks has not been previously
52 characterized for its thermal maturity and origin.

53 The scope of the present study is to examine the origin of the bitumen present within fractures and vugs
54 and its relationships to fracturing in the Late Cretaceous—Eocene oil shale of Jordan. The study has
55 three main aims:

56 (1) to define the source and emplacement history of the bitumen and test whether the bitumen is derived
57 from a local source (i.e., JOS) or has migrated from a deeper petroleum source by studying its organic-
58 geochemical characteristics;

59 (2) to better understand the transport mechanism of the bitumen into fractures and vugs; and
60 (3) to investigate whether bitumen maturation and migration coincide with fracturing, and if so, establish
61 the nature of relationships between bitumen mobilisation and fracturing.

62 Recent studies of the natural fracture systems within the JOS have shown that diagenetic processes play
63 an important role in fracture formation and distribution in the Cretaceous-Palaeogene strata of Jordan
64 (Hooker *et al.* 2017; Huggett *et al.* 2017). Hooker *et al.* (2017) presented evidence of fracture formation
65 controlled by silica diagenesis whereby fractures formed due to volume redistribution and loss
66 associated with the opal-quartz transformation during early burial. Fractures were simultaneously filled
67 by calcite. Their study demonstrated that chemical reactions can lead to open fracture pore space and
68 that the created space can be filled by diagenetic mineral phases.

69 Bitumen is present within the oil shale matrix, natural fractures and adjacent vugs in the JOS, either in
70 macroscopically visible deposits or as inclusions in the fracture cement. The geostatistical analysis of
71 fracture distribution, petrographic investigation and geochemical analyses have been carried out on
72 samples collected from 15 continuously cored sections through the JOS and selected outcrop localities.
73 The studied cored wells and the outcrop are located in central and south Jordan (Fig. 1a).

74 **The Jordan Oil Shale**

75 **Overview**

76 The JOS is an organic matter-rich, bituminous marl and limestone that was deposited in a highly
77 reducing shallow marine environment during the Maastrichtian to Late Eocene (Abed & Arouri 2006;
78 Alnawafleh 2007; Alnawafleh & Fraige 2015; Alqudah *et al.* 2015, März *et al.* 2016). Oil shale is
79 considered as Jordan's most significant natural resource. Oil shale deposits underlie more than 60% of
80 the Jordan territory, totalling ~70 billion **tonnes**. They are widespread in Jordan and can be recognized
81 in few outcrops and mostly in the subsurface. Total organic carbon (TOC) ranges from 3 to 30wt%
82 (Hakimi *et al.* 2016). The organic matter has high oil generative capacities with Hydrogen Indices
83 ranging between 600 and 900 and is characterised as a Type I/II-S kerogen due to its elevated Sulphur
84 contents of between 2-12wt% (Abed *et al.* 2005; Hakimi *et al.* 2016; Sokol *et al.* 2017; Al Aljariri
85 Alhesan 2018).

86 **Geological Framework**

87 Jordan is located along the western border of the Arabian Plate. During the Cretaceous to Eocene period,
88 the Arabian plate was part of the southern Neo-Tethys Ocean margin. The Neo-Tethys Sea periodically
89 transgressed towards the south and east, onto the Arabian Craton (Powell & Moh'd 2011). Marine
90 conditions prevailed during the Cretaceous to Late Eocene and were terminated by uplift in the Latest
91 Eocene (Fig. 1b). The area was then subjected to regional normal faulting, which was concentrated
92 mainly along pre-existing faults and zones of weakness that were reactivated in a regime of N—S
93 principal horizontal stress (Diabat & Masri 2005).

94 The major tectonic features in central Jordan include the N—S striking Dead Sea Graben/Rift valley to
95 the West, a series of E—W striking, right-lateral strike-slip faults (e.g., Zarqa Ma'in and Suwaqa Faults),
96 normal faults and grabens arranged in NW-SE direction (e.g., Azraq and Sirhan Grabens) and gentle
97 folds belonging to the Syrian Arc (Al-Zoubi & Ben-Avraham 2002; Diabat 2009; Segev *et al.* 2014).

98 The Upper Cretaceous-Eocene succession is a passive continental margin sequence changing from
99 carbonate platforms in south Jordan and open shelves in the central part to deep ramp and pelagic
100 conditions in the North (Powell & Moh'd 2011). The sedimentation and structure of Jordan were heavily
101 influenced by tectonic evolution (Abu-Jaber *et al.* 1989; Alqudah *et al.* 2015). Major syn-sedimentary
102 normal faults (NW—SE) considerably influenced the sedimentation of the JOS succession (Fig. 1c and
103 1d). The oil shale was deposited where restricted water circulation led to hypersalinity, reducing
104 conditions, and enhanced organic matter preservation (Abed *et al.* 2005, März *et al.* 2016).

105 The study area in central and southern Jordan (Fig. 1a) is covered by a sedimentary succession ranging
106 in age from the Late Cretaceous to the Eocene, which comprises three main geological formations (from
107 older to younger): Al-Hisa Phosphorite (AHP), Muwaqqar Chalk Marl (MCM) and Umm Rijam Chert-
108 Limestone (URC) (Fig. 1b). The thickness of the MCM and the URC formations gradually decrease
109 from north towards the south and southeast (Powell 1989). The three formations (AHP, MCM and URC)
110 that host the JOS, and are the focus of the present study, are overlain by the Wadi Shallala Chalk
111 Formation (WSC) and underlain by the Campanian Amman Silicified Limestone Formation (ASL) that
112 together make up the Belqa Group (Abed 2000; Powell & Moh'd 2011) (Fig. 1b). The Belqa Group
113 spans the Cretaceous/Cenozoic boundary, which is marked by a depositional hiatus in the MCM (Yassini
114 1979) (Fig. 1b).

115 The AHP Formation (Maastrichtian) mainly comprises phosphorite, phosphoritic chert and limestone,
116 chert, fossiliferous limestone (coquina) and bituminous marl. This formation contains abundant oysters,
117 bivalves, fish and reptile fragments, and foraminifera, representing a shallow-water pelagic depositional
118 environment (Powell & Moh'd 2011).

119 The MCM Formation (Maastrichtian-Eocene) consists of interbedded bituminous marl (oil shale),
120 phosphatic limestone, marly limestone and chert beds in the lower part, homogenous chalky and
121 bituminous marl in the middle part and yellowish marl, chalky marl and black chert in the upper part.

122 The phosphatic limestone, marly limestone and chert beds in the lowermost part of the MCM mark the
123 top of the AHP.

124 The URC Formation, the uppermost formation of the studied section (Fig. 2a), is composed of
125 alternating beds of chalky limestones, chalky marl, marly limestones, limestones, and abundant chert
126 beds and nodules. The chalky marl and marly limestone beds are present in the lower part of the
127 formation adjacent to the boundary with the underlying MCM formation. Carbonate concretions are
128 abundant on the boundary with the MCM formation (Fig. 2a). Shell fragments, fish teeth and bones and
129 microfossils, such as calcareous nanoplankton and foraminifera, are present in this formation. These
130 litho- and bio-facies indicate a deep-water environment of deposition of the URC formation (Powell
131 1989; Powell & Moh'd 2011; Alqudah *et al.* 2015). Both the URC and the underlying the MCM
132 formation are thicker in the North of Jordan, and they gradually decrease in thicknesses towards the
133 South and Southeast (Powell 1989).

134 **Lithostratigraphic Classification of the Studied Succession**

135 The cored intervals investigated in this study represent Upper Cretaceous through Eocene intervals of
136 the Belqa Group including the AHP, the MCM and the URC Formations (Fig. 1b and 2b).

137 The outcrop locality included in this study is an open-pit oil shale quarry (El-Lajjun), situated about 100
138 km south of Amman. The El-Lajjun quarry mainly exposes the MCM and the lowermost part of the
139 URC. The main structure in the El-Lajjun area is the El-Lajjun graben which controls a morphological
140 depression bounded to the East and West by faults striking mostly N—S (NRA 1990). The graben is
141 approximately 10 km wide and 50 m thick. Syn-tectonic sediments were deposited in the graben during
142 the Late Cretaceous—Early Palaeocene.

143 Because of the complex diachronous and repetitive nature of the oil shale interval (Alqudah *et al.* 2015)
144 (Fig. 2c), the present study subdivides the cored intervals, into three main units (Lower, Middle and
145 Upper) (Fig. 2a). The quarry section is equivalent to the most of the Middle Unit and a small part of the
146 Upper Unit. The classification is mainly based on lithotypes and the presence (Lower and Upper units)

147 or absence (Middle Unit) of chert beds/nodules as well as the enrichment of organic matter in the marl
148 beds. This classification helped to construct a composite stratigraphic section from all cores and the
149 equivalent parts in the outcrop.

150 **Lower Unit:** heterogeneous unit that is composed of phosphatic chalky marl, bituminous marl and
151 phosphatic chert with carbonate and chert concretions. Chert beds and concretions occur along
152 individual beds. They are typically 90% quartz and the remaining 10% is calcite (Huggett *et al.* 2017).
153 Chert represents 15-20% of the rock volume of this unit. Bioturbation is moderate.

154 **Middle Unit:** homogenous interval that consists of organic-rich marl, with mainly calcite cement and
155 microfossils cemented by calcite. Chert is very low within this unit. Bioturbation is high.

156 **Upper Unit:** this unit mainly composed of chalky limestone and chalky marls, with chert and silicified
157 limestone beds and concretions. Bioturbation is intense.

158 Using this lithostratigraphic classification as a framework, fractures were measured and placed in a
159 lithostratigraphic context (Fig. 2a-b).

160 It is worth to mention that the oil shales are buried to depths approaching 1000 m in the east of the
161 country (Fig. 3), where regional tilting has led to present day burial close to or at maximum burial depth,
162 whereas the western occurrences were affected by Neogene uplift and erosional unroofing, reflecting
163 maximum burial depth shallower than of those in the East (Fig. 3).

164 **Methodology**

165 **Sample Selection and Description**

166 Bitumen was investigated within fractures, vugs and the matrix of host rocks in both core and outcrop.
167 The fifteen examined cores include seven cores in the Harrana area, three in the Azraq area, two in the
168 Sirhan area, and three in the Bayer area (Fig. 1a). The cored intervals range in length from 137 m to
169 293 m per well (see supplementary Table), with a core diameter of 10cm The frequency, aperture and
170 length of the bitumen-filled fractures were described and measured in each core.

171 The quarry section provides an opportunity to analyse the horizontal distribution of bitumen fractures.
172 Bitumen-bearing fractures and their spacings were measured along horizontal scan lines (Priest &
173 Hudson 1981; Priest 1993; Bons *et al.* 2004; Zeeb *et al.* 2013).
174 Thirty-eight representative samples were collected from core and outcrop (32 samples from the fifteen
175 studied cores and 6 from the El-Lajjun exposure) and submitted for organic-geochemical and
176 petrographic analyses. The samples were taken from both bitumen-bearing fractures and their host
177 matrix. At least one fracture bitumen (FB) sample from each core was selected along with a matrix
178 bitumen (MB) sample from the host organic-rich mudrock. If bitumen-bearing fractures occurred in
179 chert or carbonate beds or concretions, matrix samples were taken from the adjacent mudstone beds (a
180 few centimeters away from concretions). The average vertical distance between fracture and matrix
181 bitumen samples is ~2 cm (see supplementary data).
182 Thin sections with a thickness of 30 μm were prepared from the fracture and matrix samples to study
183 the bitumen present within the fractures and host rock. Optical analyses of thin sections of selected
184 samples were made in cross-polarized light with a Nikon Optophot Microscope linked with a digital
185 camera. The thin sections were also examined using a FEI Quanta 650 FEG scanning electron
186 microscope (SEM). Backscattered electron (BSE) images were created to study mineral compositions
187 and textures of the samples. Elemental mapping was performed using an energy-dispersive X-ray
188 spectroscopy (EDS) attachment to the SEM. All SEM analyses were performed at 20 kV and a working
189 distance of about 10 mm.

190 **Organic Geochemistry**

191 **Methods:**

192 Geochemical analyses of the JOS, including Total Organic Carbon (TOC) and Total Sulphur (TS), were
193 performed using a LECO elemental analyser. Rock Eval pyrolysis was used to characterize the type and
194 maturity of the organic matter using a Vinci Rock-Eval 6 Analyser.

195 Twenty-four samples (22 from cores and 2 from the exposure) were selected for extract analyses. Rock
196 samples were prepared by rinsing with distilled water and dichloromethane (DCM). The bitumen was
197 extracted from samples drilled out of fractures/vugs and rock matrix using a standard Soxhlet Extraction
198 technique (Mueller & Philp 1998). Briefly, pulverized and weighed samples were loaded into Soxhlet
199 extractors containing a 3:1 mixture of DCM and Methanol (CH₃OH; abbreviated here MeOH) and
200 extracted for 24 hrs, then blown down under N₂ gas. Asphaltenes, which represent a substantial fraction
201 of the extract, were precipitated from the whole extract using an excess of hexane (Aske *et al.* 2001).
202 The samples were then centrifuged at 5000 rpm, and the supernatant solution of each sample,
203 representing the maltene fraction, was carefully transferred into a separate glass vial and blown down
204 to about 0.5 ml by N₂ gas. Elemental Sulphur was removed using activated copper prior to column
205 chromatography.

206 The extracts were passed through a column containing silica gel to remove any remaining water, before
207 being separated by alumina (Al₂O₃) column chromatography. The extract sample was eluted
208 sequentially by hexane/DCM (9:1, v/v) and DCM/MeOH (1:1, v/v) to separate aliphatic and aromatic
209 fractions respectively.

210 Biomarkers from the maltene fraction were analysed using an Agilent 5977B GCMS. The GC oven
211 program was set to 80 °C for 1 min, then increased to 130 °C at 20 °C/min, and then to a maximum
212 temperature of 325 °C at 10 °C/min where it was held for 30 min. Triterpane and sterane biomarkers
213 were identified from the maltene fraction with the standard methods using m/z 191 and m/z 217
214 fragmentograms run in SIM mode. The biomarker results were compared to an internal standard
215 (SRM2266). Identification of biomarkers was carried out based on the retention time.

216 **Results**

217 **Fracture Description**

218 **Fracture Types and Mineralization**

219 A wide range of structures were observed and measured from the core and outcrop. These include veins
220 (cemented fractures), joints (uncemented fractures), cone-in-cone structures, faults (fractures with

offsets), and dilatational breccias. Cemented veins include both mineralized and bitumen-filled veins. Opening-mode fractures (veins and joints) are the most dominant fracture type observed in the core and outcrop (Fig. 4a). Shear fractures are counted as faults.

At the core scale, veins are the most abundant fracture type observed (Fig. 4a). They are identified by the distinct colors of their filling materials. They are sealed by different types of cements including calcite, silica (as quartz or chalcedony), and bitumen. Most of the opening-mode fractures observed in the core are planar; however, a considerable number are folded (compacted) veins (Fig. 4b). These folded veins are filled by calcite and are interpreted by Hooker *et al.* (2017) to be deformed by sediment compaction after early emplacement.

Bitumen is either present within the mineralized veins, or entirely fills fractures and vugs. Fractures entirely filled by bitumen are referred to here as bitumen veins (BVs) (Fig. 5b and 5d-g). Bitumen is only found within the planar veins; no observations were documented of bitumen within folded calcite veins (FCVs). Bitumen in unfolded calcite veins (BCVs) is observed either as solid inclusions within the cement or as fillings of the remaining porosity and inter-crystalline pore space (Fig. 5a and 5c). No crosscutting relationships between calcite veins and bitumen veins were documented.

Neither is bitumen found in silica-cemented veins (SVs), but BVs are observed to crosscut SVs (Fig 5f and 6a-b, and some BVs exploit the preexisting SVs by running immediately adjacent and parallel to SVs (BSVs) (Fig. 6a-b). These observations establish that the timing of BVs post-dates the SVs.

There are many examples in the cores of horizontal BCVs crosscutting early folded calcite veins (Fig. 6f-g), but BCVs and BVs have not been observed crosscutting each other. Importantly, no systematic crosscutting relationships are observed between horizontal BVs and vertical BVs. This suggests that all geometries and types of bitumen-bearing fractures are coeval.

There are only a few observations of bitumen inclusions associated with shear fractures (faults), such as observed in the lower unit of core 7 at a depth of 667 m. These few cases mainly represent bitumen that occurs within the fault cement or in opening-mode fractures that are associated with fault damage zones.

246 Fractured beds are predominantly those cemented by carbonate and silicate minerals (Huggett *et al.*,
247 2017). Fracture cements generally reflect the lithology of the host unit such that calcite veins are
248 observed in calcareous mudstones and limestones whereas chalcedony and silica veins are present in
249 silicified/chert beds.

250 In the quarry section, only BVs are observed, and they are confined to the oil shale beds. No mineralized
251 veins containing any form of bitumen were observed in the quarry (i.e., no BSVs, BCVs).

252 **Fracture Orientation, Geometry and Aperture**

253 The majority (>70%) of the bitumen-bearing fractures (BVs and BCVs) observed in the cores are sub-
254 vertical to vertical (Fig. 5a-c and 6c-d). The dip angles of most vertical bitumen-bearing fractures
255 observed in the core vary with the change in lithology chert and carbonates beds/concretions (Fig. 5a,
256 5d and 6e). Due to the unknown orientation of the core, the true fracture strike was not constrained in
257 this study. Horizontal fractures (bedding-parallel) and a combination of horizontal and vertical fractures
258 forming complex fracture networks also occur (Fig. 5f and 6f-g).

259 Vertical bitumen-bearing fractures in the cores range from 1 to 120 cm in height (parallel to the core
260 axis), whereas the length of bed-parallel fractures (orthogonal to core axis) is not measurable due to the
261 limited core width. Vertical core fractures measured within the homogenous organic-rich marl unit
262 (Middle Unit), have smaller apertures and greater heights than fractures within the heterogeneous units
263 (Lower and Upper units), which are commonly restricted vertically by chert and silicified bands. BVs
264 cut across their host beds or concretions entirely (Fig. 5b, 5d-g and 6a-e).

265 BVs are less strictly planar (more irregular) than other mineralized veins (i.e., CVs and CVs) and
266 bitumen-bearing fractures (i.e., BSVs and BCVs) (Fig. 5d-g and 6d-e). Bitumen-bearing fractures show
267 a range of tip morphologies varying from single tapering ends to branching ends (Fig. 5 and 6).
268 Individual thick BVs commonly branch, particularly within mudstone beds (Fig. 6e). BVs tend to have
269 larger apertures in the chert, silicified and carbonate beds or concretions than in the mudstone (Fig. 5d-

270 f, and 6d-e). Both BCVs and BVs tend to deflect in their trajectory when crossing different lithofacies
271 (Fig. 5a, 5d, and 6e).

272 Generally, BVs have larger aperture sizes than other bitumen-bearing fractures (Fig. 6d-e). The
273 maximum aperture size of BVs averages 0.90 cm while it averages 0.40 cm for BCVs. BVs display
274 apertures that are variable along fracture traces (Fig. 6d-e). In all types of bitumen-bearing fractures,
275 fracture aperture decreases in a fairly regular taper towards the tips (Fig. 5a-g and 6a-c).

276 BVs observed in the El-Lajjun quarry are planar and exclusively vertical (Fig. 6c). They range in height
277 from 5 cm to 20 cm and have a mean maximum aperture of 0.20 cm. The veins in outcrop do not exhibit
278 any branching features that are comparable to the BVs observed in the cores.

279 **Fracture Intensity and Distribution**

280 Bitumen-bearing fractures are found dominantly in the lower section of in all cores, which comprises
281 organic-rich mudstones interbedded with silicified units or chert beds/nodules (Fig. 2). The majority of
282 bitumen-bearing fractures in the lower unit are confined to silicified, chert and carbonate
283 beds/concretions positioned between un-fractured, organic-rich mudstone beds particularly those
284 mudstone beds with higher contents of TOC and S (Fig. 2b; Table 1).

285 Generally, BVs are highly interconnected in the core; it is difficult to find individual BVs that do not
286 intersect others (Fig. 5d, 5f and 6e). Other bitumen-bearing fractures are commonly observed as singular
287 fractures (Fig. 5a, 5c and 6d). Both horizontal and vertical bitumen-bearing fractures are observed within
288 the Lower Unit; however, horizontal fractures are less abundant than vertical fractures and 90% of them
289 are only filled by bitumen (as BVs).

290 BVs are closely spaced in the core and tend to cluster. This clustering increases the chance of observing
291 them within the limited core width and may explain the high intensity of BVs compared to other
292 bitumen-bearing fractures that might have a wider fracture spacing that exceeds the core width.

293 The frequencies and cumulative lengths of all bitumen-bearing fractures were normalized to the length
294 of recovered core (Fig. 2). The data reflect high intensities of bitumen-filled fractures and vugs with the

295 progressive increase of the present-day depth (Fig. 2 and 3a-b). A few BVs (5 % of total bitumen
296 fractures) are observed in the middle unit in the homogenous organic-rich mudstones that lack chert.
297 Bitumen-bearing fractures are more abundant in the Azraq cores (CE Jordan) than the Harrana cores
298 (CW Jordan) (Fig. 3a-b). This increase in abundance eastwards may reflect the greater maximum burial
299 depth (Fig. 3b). The intensity of bitumen fractures in the lower unit of the core in the East is more
300 than double the intensity in the same unit in the West.

301 Bitumen fractures are also observed in the outcrop at the El-Lajjun quarry within the lower part of the
302 MCM formation confined to a 20-cm thick organic-rich oil shale bed (Fig. 6c). The quarry allowed a
303 3D visualization of bitumen-bearing fractures and their horizontal distribution. The fractures heights are
304 mostly equal to the bed thickness. The average fracture spacing of the measured fractures is 12 cm.

305 **Petrographic Description of Host Rock and Bitumen-Bearing Fractures**

306 Petrographic examination revealed a wide variety of host rock lithologies, fracture cements, textures
307 and crosscutting relationships. This demonstrates a complex history of deposition, fracturing and
308 sealing. It also allowed characterisation of the microscopic occurrences of bitumen and its migration
309 pathways.

310 Petrographic investigation of both the lower unit, which is the host of most of the bitumen-bearing
311 fractures, and the middle unit shows that the mudstone mainly consists of calcite, quartz, organic matter
312 (bitumen) and apatite, with locally considerable amounts of chalcedony, dolomite, and occasionally
313 pyrite (Huggett *et al.* 2017). Clay is only rarely observed and quartz is commonly of microcrystalline
314 nature. Calcite has cemented most microfossils and radiolaria are locally abundant.

315 The interbedding of chert and mudstone in the lower unit is believed to be the result of diagenetic
316 alteration of locally abundant concentrations of radiolaria and diatoms (Hooker *et al.* 2017). The chert
317 is believed to have developed by replacing carbonate components in the original host material with silica
318 from biogenic components (Hooker *et al.* 2017; Huggett *et al.* 2017). This is consistent with the low
319 silica content of the adjacent mudstones.

320 Bitumen is observed as small amorphous particles in variable shapes and as flakes that are present in
321 the matrix of the organic-rich mudstones (oil shale) in both the lower and middle units (Fig. 7c-d).

322 Fracture bitumen under the microscope is observed to either entirely fill the fracture (i.e., bitumen in
323 BVs; Fig. 7c and 7f), or to be texturally enclosed by calcite cements (i.e., in BCVs; Fig. 7a). BCVs are
324 characterized by a crack-seal texture (e.g., Ramsay 1980), **represented by** multiple generations of
325 calcite crystals with elongate-blocky morphology (Fig. 7a). The veins appear under the microscope as
326 multiple parallel bands of cements. The crack-seal texture indicates that calcite precipitation was
327 synchronous with fracture opening. Micro-bitumen inclusions (sub-millimetre-scale) and inclusions of
328 organic-rich host-rock are present within the cement of these calcite veins (Fig. 7a-b) which indicates
329 that bitumen was present during formation of the veins. Bitumen filling the vacant segments of partially-
330 filled BCVs appears to have similar petrographic properties to the bitumen within the calcite cement.

331 Bitumen micro-veins (BMVs) are observed in internally branching networks, resulting in incipient
332 brecciation of the organic-rich mudstone (Fig. 5g, and 7f-g). Horizontal and sub-horizontal
333 microfractures entirely filled by bitumen are also commonly observed within the organic-rich mudstone
334 (Fig. 7c). This microfracturing is observed particularly around or at the margin of calcite and pyrite
335 crystals (Fig. 7c-d).

336 Microscopic examination of FCV shows that these early veins do not contain any traces of bitumen but
337 are entirely cemented by calcite. This indicates that bitumen generation and migration postdate the
338 development of folded veins. It also strongly supports the macroscopic observations described above
339 from the core.

340 BVs exhibit a clear crosscutting relationship with SVs at the microscale but not with BCVs. Importantly,
341 the silica cement in SVs is entirely free of bitumen inclusions. BMVs with varied directions were
342 observed, including vertical BMVs, horizontal BMVs and network BMVs. However, no crosscutting
343 relationships between horizontal and vertical BMVs were detected.

Organic Geochemistry

Source Rock Characterization

Geochemical properties of the JOS samples are presented in Table 2. The JOS has high TOC values ranging from 6 to 30 wt% and S contents from 1.5 to 8.3 wt%. Hydrogen Index (HI) values range from 583 to 880 mg HC/g TOC, indicating excellent oil-prone kerogen. The Tmax values range from 389 to 424 °C (<0.6% VR/E), and the Production Index (PI) has an average of about 0.03 mg/g TOC, both parameters indicating a thermally immature source rock (Fig. 8). The low maturity of the JOS indicates that regional maximum palaeo-burial depths were likely shallow (few hundred metres), or more accurately, palaeo-burial temperatures were low (~ 30-50 °C).

Biomarkers of Fracture and Matrix Bitumens

Table 3 lists pertinent characteristics of the m/z 191 (Triterpenoids) and 217 fragmentograms (Steranes) from extracts of both fracture (FB) and matrix bitumen (MB). The most prominent feature of the triterpane fragmentogram is the high concentration of gammacerane (Fig. 9a-b), which is an indicator of water column stratification possibly due to salinity variations (Mello *et al.* 1988; Sinninghe-Damste *et al.* 1995, Peters *et al.* 2005). C29:C30 $\alpha\beta$ hopane ratios range from 0.27-0.60 and gammacerane: C30 $\alpha\beta$ hopane ratios from 0.34-0.93. The 22S/(22S+R) C₃₁ $\alpha\beta$ extended-hopane ratio ranges from very immature values of 0.2 to the equilibrium value of 0.6 (Peters *et al.* 2005).

Sterane biomarkers are commonly used to indicate depositional environments and organic matter biomass input (Huang & Meinschein 1979; Seifert & Moldowan 1981; Volkman 1986; Peters *et al.* 2005). Table 3 lists the relative amounts of the C27, C28 and C29 $\alpha\alpha\alpha$ R steranes, which are the predominant isomers in all the samples. The samples all show a predominance of C27 steranes (47-58%), with subequal amounts of C28 and C29 steranes comprising the rest (Fig. 9c-d, and 10). All the samples, both matrix and bitumen, cluster in a relatively small area in Fig. 10, indicating very similar biomass contributions to the kerogen of the JOS (Huang & Meinschein 1979; Seifert & Moldowan 1981; Volkman 1986; Peters *et al.* 2005).

369 20S/(20S+20R) $\alpha\alpha\alpha$ and the $\alpha\beta\beta/(\alpha\beta\beta+\alpha\alpha\alpha)$ C28 sterane ratios range from 0.25-0.52 and 0.41-0.66
370 respectively set (Table 3; Fig. 11a). Most of the samples have yet to reach the equilibrium maturity
371 values for these maturity parameters of 0.55 and 0.7, respectively, and attest to their low maturity.

372 **Discussion**

373 **Source and Maturity of Fracture Bitumens**

374 The JOS bituminous and organic rich marls comprise an excellent oil prone source rock. The presence
375 of Type I/II-S kerogens indicates high quality organic matter type that is able to generate low API
376 gravity, asphaltene-rich bitumen at relatively low thermal stress because of the high sulphur (1.5-
377 12wt%) contents (Burnham 2017).

378 The biomarker data obtained from the matrix and fracture bitumens from the JOS indicate that they are
379 sourced from the same type of organic matter. Subtle variations in biomarker parameters (e.g., C29/C30
380 hopane, gammacerane/hopane and the sterane carbon number distributions) between wells probably
381 reflect slight geographic differences in environment of deposition and biomass input. Although a
382 detailed discussion of the formation of these source rocks is beyond the scope of this paper, the pertinent
383 point is that there is a close similarity in the biomarker patterns of the matrix bitumen, and the solid
384 bitumen found in fractures and vugs (Fig. 9 and 11). Most compelling are the maturity-related hopane
385 and sterane isomerization parameters (e.g., hopane 22S/(22S+22R), and sterane 20S/20S-20R) and
386 $\alpha\beta\beta/(\alpha\beta\beta+\alpha\alpha\alpha)$ parameters) that are remarkably similar between matrix and fracture bitumen and
387 indicate low thermal levels of stress, which is also consistent with bulk Tmax values that point to low
388 thermal maturity (0.5-0.6% VRE). These lines of evidence strongly suggest that both matrix and fracture
389 bitumen is locally derived and indigenous to the JOS and has migrated at most on the scale of a few
390 beds, i.e., cm-scale to m-scale migration. This applies to both fractures and vugs hosted in the
391 bituminous marls and to those that extend into adjacent chert and carbonate beds which inherently have
392 little or no organic matter.

393 Samples from Core 6 and the quarry show the lowest levels of maturity for the matrix and fracture/vug
394 bitumens (Fig. 11a), suggesting the least amount of burial/thermal stress for these localities. This is
395 consistent with their shallow present day burial depth, and likely minimum maximum burial depth
396 relative to their counterparts in the eastern part of the basin (Fig. 3).

397 **Bitumen Generation and Migration**

398 The elevated TOC and sulphur contents of the JOS are considered here to be the prime factor in the
399 relatively early mobilisation of a bitumen phase. Although the JOS is immature by conventional
400 standards of thermal maturity, the high total content of sulphur up to 8 wt% analysed in the present study
401 (Table1) and up to 12 wt% in other studies (e.g., Al Aljariri Alhesan 2018), is interpreted to have
402 contributed to early cracking of the Type I/II-S kerogen, resulting in the generation of bitumen
403 (Burnham 2017).

404 Hydrocarbon migration out of the source rock is usually considered as the explanation for the presence
405 of solid bitumen in veins (Parnell & Carey 1995; Fink *et al.* 2016). In the case of the JOS, the presence
406 of solid bitumen within matrix, fractures and vugs within the main source interval is attributed to very
407 short distance (mm- to m-scale) hydrocarbon migration through fractures and vugs.

408 The early-generated bitumen appears to have been squeezed out and mobilised not by buoyancy forces
409 (as with some views of primary hydrocarbon migration), but under the vertical load imposed during
410 peak burial. Following the recent model of Pepper (2017), it is suggested that the transformation from
411 the kerogen to the bitumen phase generated an overpressure (i.e., by fluid volume increase) that was
412 equivalent to the overburden stress and enabled the bitumen to migrate via newly propagating fracture
413 pathways through the host organic-rich mudstone beds. This process is different from the conventional
414 notion of primary migration where hydrocarbons saturate available pore spaces before being expelled
415 into carrier beds. Instead, these rocks have extruded early-generated heavy bitumen under the
416 overburden load and led to redistribution into vugs and pre-existing (BCVs) or newly-forming fractures.

417 The presence of early-generated bitumen in the pores of the low-permeability mudrocks has built up
418 overpressure that triggered new fractures (BVs) to create.

419 The difference in physical and mechanical rock properties of the chert, carbonate and mudstone beds in
420 the host source rock interval can be viewed as a form of mechanical stratigraphy (cf. Gross 1995). This
421 interbedding of contrasting rock types may have exerted a second order control on the bitumen migration
422 in that local stress concentrations (e.g., around chert and carbonate nodules) may have promoted
423 fracturing at bed boundaries that could be exploited by the mobilised bitumen. It is also likely that the
424 overpressure within the bitumen phase was instrumental in driving fracture propagation, as indeed
425 implied by the prevalence of both vertical and horizontal bitumen veins (cf. Mandl & Harkness 1987).

426 Following expulsion of bitumen by mechanical compaction when the load-bearing capacity of the source
427 rocks was exceeded, the resulting volume decrease of the rocks caused overpressure that allowed the
428 bitumen to migrate only short (cm-scale) distances from the saturated mudstone (oil shale) beds towards
429 the adjacent silicified, chert and carbonate beds or concretions via networks of newly propagating
430 bitumen-bearing fractures (Fig. 6d-f and 12). This situation is considered as a good indication of bitumen
431 expulsion resulting from mechanical compaction once the bitumen phase achieved load bearing capacity
432 and is seen, for example, through a low-organic content mudstone zone on the contact with the chert or
433 carbonate beds/concretions (see Fig. 5b and 5e). It indicates that the compaction-related pressure has
434 allowed the migration of the low-maturity bitumen generated from the local kerogen and squeezed it,
435 creating fractures (Fig. 12).

436 Furthermore, the strongly comparable geochemical signatures of the fracture and matrix bitumen are a
437 robust indication of local migration (cm-scale) of bitumen from the saturated mudstone (organic-rich
438 oil shale) towards the brittle chert and carbonate intervals (Fig. 8, 10 and 11). Petrographic observations
439 (Fig. 7f) show that the direction of fracture propagation is from the organic-rich mudstone beds towards
440 the chert or carbonate concretions. The pathways taken by migrating bitumen from outside carbonate
441 concretions directed inward to their interiors is also evident in microscopic observations (Fig. 7f).

Development of Bitumen-bearing Fractures

Distribution of Bitumen-Bearing Fractures

The vertical distribution of bitumen-bearing fractures in the cores is influenced by two main factors. In the lower unit of all cored successions, the fracture intensity shows a positive correlation with TOC and TS (Fig. 2c). This observation is consistent with the model presented in the previous section for local bitumen generation and mobilisation during early catagenesis since the fracture intensity would be expected to be greatest where the concentration of kerogen is highest. It is interesting to observe that fracture intensity also correlates with TS, which is consistent with the arguments presented above that it is the high sulphur contents that allows very early bitumen generation.

The second factor is the gross burial history and thermal stress that the source interval experienced. The high intensity of bitumen-bearing fractures in the lower unit of the cores when compared to the overlying two units (middle and upper units) indicates that burial depth plays a role in the development of these fractures. The overall increase in fracture intensity of the lower fractured interval from West to East (Fig. 3a-b) is another indicator that increased maximum burial in the East and enhanced thermal stress and peak temperatures play a role in fracture formation.

At the bed scale, bitumen-bearing fractures are mainly observed clustering in the chert and silicified beds, positioned between or beneath organic-rich beds in the lower unit. This predominance of bitumen-bearing fractures in layers with high rock stiffness indicates that the development of bitumen fractures has been primarily controlled by the physical and mechanical properties of the rock, represented by the small-scale mechanical stratigraphy. Rapid vertical changes in Poisson's ratio have been suggested as a means for localising mode 1 fracture development (Teufel & Clark 1984; McDermott *et al.* 2013), and such a mechanism could apply here.

Fracture analysis of the outcrop analogue provided some constraints on possible horizontal distribution of BVs in the middle unit, which in the core has very low fracture abundance. The average fracture spacing at outcrop was c. 12 cm which is almost double the typical core diameter, and thus fracture

467 intensity in the middle unit from core observation is certainly significantly underestimated (cf. Alfahmi
468 2018).

469 **Timing of Bitumen-Bearing Fractures**

470 Cross-cutting relations are critical for constraining the timing of fractures (Beaudoin *et al.* 2015; Hooker
471 *et al.* 2018). The lack of systematic cross-cutting relationships between the different types of bitumen-
472 bearing fractures leads to the conclusion that these fractures were developing coevally during the period
473 of active bitumen generation. BCVs and BVs seem to have crosscut all other type of fractures except
474 for late calcite veins; suggesting that BCVs and BVs postdate all opening-mode fractures (i.e., SVs and
475 FCVs) present in the studied succession and are coeval with late calcite veins (Fig. 6c and 6f-g). The
476 crosscutting relationship between vertical BVs and SVs indicates that both the BCVs and BVs postdate
477 silica diagenesis. The absence of any crosscutting relationships between vertical and horizontal BVs in
478 the core and at the microscale implies a synchronicity in the development of both the horizontal and
479 vertical BVs, and this in turn points to the development of a lithostatic overpressure in the bitumen phase
480 (cf. Mandl & Harkness 1987).

481 At the microscale, the presence of bitumen inclusions within the cement of the planar calcite veins (i.e.,
482 BCVs), indicates that bitumen was present during the opening and sealing of the vein. This suggests
483 that bitumen migration coincides with the formation of calcite veins. The crack-seal pattern of BCVs
484 further indicates that calcite precipitation was synchronous with opening of the fracture. Similar
485 arguments were advanced for the co-existence of bitumen and saturated mineralising pore fluids by
486 Parnell and Carey (1995).

487 The late development of bitumen-bearing fractures (cf. Hooker *et al.* 2017) is consistent with the model
488 presented above for bitumen mobilisation at the peak of thermal stress, i.e., at a late stage in the burial
489 history prior to any uplift and cooling.

490 **Formation Mechanisms of Bitumen-Bearing Fractures**

491 Generally, opening-mode fractures propagate along a plane perpendicular to the minimum-compressive
492 principal stress, normal to the plane of the crack (Secor 1965). One mechanism for their formation is
493 hydraulic fracturing, where a pore pressure exceeds the least compressive total normal stress, but they
494 may also form at pore pressures significantly less than the overburden stress and by minor extensional
495 or volumetric strains, or thermal stresses, particularly under shallow burial conditions (Eichhubl *et al.*
496 2001; Eichhubl & Aydin 2003; Olson *et al.* 2009).

497 Veins are considered as important structural elements since they reflect stages of geological activity that
498 occurred after formation of the host unit (Bons *et al.* 2012). According to Hooker *et al.* (2017), calcite
499 cement in the different types of calcite veins present in the JOS has been formed at many different phases
500 during both burial and uplift of the host units. The high percentage of calcite veins in the calcareous,
501 organic-rich oil shale relative to all opening-mode fractures suggests the circulation of calcium
502 carbonate-rich fluids in the fracture networks.

503 Calcite veins are considered here to be formed by three possible fracture-forming mechanisms. These
504 include diagenetic processes, tectonic stresses or fluid overpressure. The investigated bitumen-bearing
505 fractures are coeval with late planar calcite veins which are believed to be tectonic-related fractures
506 (Hooker *et al.*, 2017). The BCVs identified in the present study have elongate-blocky textures which
507 reveal a moderate crack opening rate according to Prajapati *et al.* (2018). Elongate-blocky crystals
508 demonstrate preferred orientations at the final phase of growth, indicating the presence of growth
509 competition during vein development (Hilgers & Urai 2002; Prajapati *et al.* 2018).

510 The sealing of BCVs shows overlapping filling stages. This is evidenced by the occurrence of bitumen
511 within the crack-seal structure which suggests that the bitumen occurrence is syngenetic with the
512 cementation of calcite veins (see Fig. 7a-b) (cf. Parnell & Carey 1995). The crack-seal texture implies
513 incremental opening and sealing. This internal structure of these veins indicates that the calcite has
514 started to precipitate in the fracture, and the bitumen filled the remaining porosity and the vacant

515 segments before the fractures were entirely sealed. A process similar to this was proposed in a study of
516 the Woodford Shale by Comer (2007).

517 The folded calcite veins are free of any bitumen traces and are thought to have formed during early
518 burial in response to silica diagenesis and were folded by sediment compaction (Hooker *et al.* 2017).

519 Planar SVs are also thought to have formed early due to silica diagenesis. The sequence of events of all
520 these fractures cements is summarized in Fig. 13 (Hooker *et al.* 2017).

521 Low permeability and high organic content play a key role in fracturing (Mandl & Harkness 1987). The
522 development of bitumen-bearing fractures appears to have been controlled (for BVs) or at least have
523 been assisted (for BVCs) by hydraulic fracturing, driven by lithostatic fluid overpressure in the organic
524 material. Brecciation in the organic-rich mudstone, particularly mosaic brecciation (see Fig. 5g, and
525 5g), can be indicative of hydraulically-fractured rock due to fluid overpressure within this low-
526 permeability unit (Parnell & Carey 1995; Passchier 2000). The bitumen-supported breccia in the
527 mudstone reflects a pressure regime that has been hydrostatic and then developed to highly elevated
528 overpressured led to fracture (i.e., brecciation) the host mudstone (Parnell & Carey 1995).

529 The bed-parallel BVs and BVCs present within the organic-rich oil shale (see Fig. 6c and 6f-g) show a
530 good example of hydraulic-fracturing produced by bitumen overpressuring in which the bitumen pore
531 pressure exceeds the vertical stress generated by the overburden load. The hydraulic fracture usually
532 occurs when the Mohr circle touches the failure envelope. The size of Mohr circle is governed by
533 effective stress (σ^-), which is represented by the difference between total stress (σ) and fluid pressure
534 (pF):

535
$$\sigma^- = \sigma - pF \quad (1)$$

536 At the microscopic scale, the development of bitumen filaments in well-developed microfractures
537 (BMVs) within the organic-rich mudstone beds also indicates fracturing due to high pore pressure
538 (Fig. 7c). These BMVs that propagate within and around calcite and pyrite crystals, are interpreted to

539 have been generated by fluid pressure in the bitumen phase (pB) that exceeded the vertical stress (σv):

540
$$pB > \sigma v \quad (2)$$

541 Fracturing driven by fluid overpressure relating to maturation of organic matter has been documented
542 in a range of studies (e.g., Jochum *et al.* 1995; Zhang *et al.* 2016; Meng *et al.* 2017). It is often suggested
543 that volume expansion of kerogen during thermal maturation is the main driver for fracturing (Michels
544 *et al.* 1994; Figueroa Pilz *et al.* 2017). In the case of the JOS, the generated bitumen is of early maturity.
545 However, the yield of this early expelled bitumen seems to have been high enough to cause a volume
546 change that resulted in fracturing.

547 The stiffness of chert and silicified beds is argued to have directed the fracturing to be straighter and
548 with bigger apertures than in the ductile mudstone; emphasising the role of the rock properties in
549 fracturing and aperture development.

550 The aperture irregularity of BVs in silicified and chert beds (Fig. 6d-e), the deflection of veins when
551 they propagate in different beds (Fig. 5a, and 6e) and the branching and splaying of BVs in mudstone
552 (Fig. 6e) all indicate that the fracturing generated by fluid overpressure was controlled by the rock
553 properties (Bons *et al.* 2012). The veins seem to have been able to branch or change direction due to the
554 ductility of the mud rocks, presenting further evidence of fracture formation due to fluid overpressure.
555 Therefore, we argue that in the low-permeability mudstone beds, the bitumen overpressure has forced
556 the mudstone to fracture or brecciate. This is consistent with the study of Parnell & Carey (1995).

557 A final line of evidence for overpressured bitumen acting as a fracture driver comes from the observation
558 that a single BV can propagate through three types (mudstone, chert and carbonate) of rocks with
559 different mechanical properties (Fig. 5d). This is also supported by microscopic observations where BVs
560 and MBVs propagate from an organic-rich mudstone bed towards a carbonate concretion (see Fig. 7f).
561 The microscopic occurrence of bitumen within the matrix in both the lower and middle units of the core
562 indicates that the bitumen has been subjected to an external pressure that forced this *in-situ* bitumen to
563 find a way to release this pressure by generating fractures in the low permeability mudstone matrix.

564 **Conclusions**

- 565 (1) The biomarker and petrographic results of fracture and matrix bitumen from 15 cores and one
566 outcrop of the JOS show that the source of bitumen within fractures and adjacent vugs are very
567 low-mature hydrocarbons expelled from the JOS matrix, and have not migrated from another
568 petroleum source.
- 569 (2) Maturity indicators imply that the oil shale is everywhere in the very early-oil generation stage,
570 but with a regional variation from west to east resulting from greater maximum burial depth.
- 571 (3) The present study has revealed that bitumen fractures developed by hydraulic fracturing as the
572 result of fluid overpressure in the organic matter due to permeability destruction in the organic
573 mudstones which prevents fluid loss. Overpressured bitumen has acted as a fracture driver,
574 generating bitumen veins in both the organic-rich mudstones and the adjacent chert and silicified
575 intervals.
- 576 (4) Rock properties played an important role in the distribution of bitumen-bearing fractures with
577 High intensities of bitumen-bearing fractures occurring in chert and silicified beds.
- 578 (5) Late calcite veins contain bitumen inclusion (BCVs) which shows that bitumen occurrence is
579 syngenetic with the cementation of calcite veins, and was generated relatively late in the
580 paragenetic sequence.

581 **Acknowledgment**

582 This research is a part of a PhD project being conducted by Israa S. Abu-Mahfouz as a part of the
583 "Fractures in Mudrocks" theme under the Shell-Oxford collaborative agreement. We thank the Jordan
584 oil shale company (JOSCO) for providing the core data and samples. We thank Lauren O'Connor,
585 Alexander Dickson, Jon Wells, and Stephen Wyatt for helping with the laboratory preparations.

586 **Funding**

587 This research is co-funded by Royal Dutch Shell PLC, represented by JOSCO, and the University of
588 Oxford.

589 **References**

- 590 Abed, A.M., 2000. The Geology of Jordan and Its Environment and Water (in Arabic). Publication of the
591 Jordanian Geologists Association, Amman
- 592 Abed, A.M., & Al-Arouri, K. 1994. Organic Geochemistry of Central Jordan Upper Cretaceous Phosphorites:
593 Phosphogenesis and Source Rock. Proceedings of the 2nd International Conference-Geology of the Arab
594 World, Cairo University, Cairo, 321-338
- 595 Abed, A.M., Arouri, K.R. & Boreham, C.J. 2005. Source rock potential of the phosphorite bituminous chalk-
596 marl sequence in Jordan, Mar. Pet. Geol., v. 22. p. 413–425
- 597 Abed, A.M. & Arouri, K. 2006. Characterization and Genesis of Oil Shale from Jordan. International
598 Conference on Oils Shale, University of Jordan, Amman, Jordan
- 599 Abed, A.M., Arouri, K., Amiereh, B.S. & Al-Hawari, Z. 2009. Characterization and Genesis of Some Jordanian
600 Oil Shales. Dirasat. Pure Sciences, v. 36, p. 7-17
- 601 Abu-Jaber, N.S. Kimberly, M.M. & Cavaroc, V.V. 1989. Mesozoic-Paleogene basin development within the
602 eastern Mediterranean borderland: J. Pet. Geol., v. 12, p. 419-436
- 603 Al-Bahlani, A.M.M. & Babadagli, T. 2009. Laboratory and Field Scale Analysis of Steam Over Solvent
604 Injection in Fractured Reservoirs (SOS FR) for Heavy Oil Recovery. Presented at the SPE Annual Technical
605 Conference and Exhibition, New Orleans, 4-7 October. SPE-124047-MS, <http://dx.doi.org/10.2118/124047-MS>
- 606 Al-Bahlani, A. M. & Babadagli, T. 2011a. Field scale applicability and efficiency analysis of Steam-Over-
607 Solvent Injection in Fractured Reservoirs (SOS-FR) method for heavy oil recovery. J. Pet. Sci. Eng. v. 78 (2):
608 p. 338-346, <http://dx.doi.org/http://dx.doi.org/10.1016/j.petrol.2011.07.001>
- 609 Al-Bahlani, A. M. & Babadagli, T. 2011b. Steam-over-Solvent Injection in Fractured Reservoirs (SOS-FR)
610 Technique as a New Approach for Heavy-Oil and Bitumen Recovery: An Overview of the Method: Energy
611 Fuels, v. 25 (10): p. 4528-4539. <http://dx.doi.org/10.1021/ef200809z>
- 612 Alfahmi, M.M. 2018. Controls on fracture abundance in gently deformed carbonates, PhD thesis, University of
613 Oxford, Oxford, 318 p

614 Aljariri Alhesan, J., Fei, Y., Marshall, M., Jackson, W., Qi, Y., Chaffee, A., & Cassidy, P. 2018. Long time, low
615 temperature pyrolysis of El-Lajjun oil shale. *Journal of Analytical and Applied Pyrolysis*, v. 130, p. 135-141,
616 <https://doi.org/10.1016/j.jaap.2018.01.017>

617 Ali Hussein, M., Alqudah, M., Podlaha, O.G., van den Boorn, S., Kolonic, S., & Mutterlose, J. 2014a.
618 Ichnofabrics of Eocene oil shales from central Jordan and their use for paleoenvironmental reconstructions.
619 *GeoArabia*, v. 19 (1), p. 143–158

620 Ali Hussein, M., Alqudah, M., Van den Boorn, S., Kolonic, S., Podlaha, O.G., & Mutterlose, J. 2014b. Eocene
621 oil shales from Jordan- their petrography, carbon and oxygen stable isotopes. *GeoArabia*, v. 19, (3), p. 139-162

622 Alnawafleh, H.M. 2007. Geological Factors Controlling the Variability of Maastrichtian Bituminous Rocks in
623 Jordan, PhD Thesis, The University of Nottingham, Nottingham.

624 Alnawafleh, H. M. & Fraige, F.Y. 2015. Analysis of Selected Oil Shale Samples from El-Lajjun, Central
625 Jordan. *Geomaterials*, v. 5, p. 77-84, <http://dx.doi.org/10.4236/gm.2015.53008>

626 Alqudah, M., Ali Hussein, M., Van den Boorn, S. Podlaha, O., & Mutterlose, J. 2015. Biostratigraphy and
627 depositional setting of Maastrichtian – Eocene oil shales from Jordan. *Marine and Petroleum Geology*, v. 60, p.
628 87-104, <https://doi.org/10.1016/j.marpetgeo.2014.07.025>

629 Al-Zoubi, A., & Ben-Avraham, Z. 2002. Structure of the earth's crust in Jordan from potential field data.
630 *Tectonophysics*, v. 346, p. 45-59

631 Aske, N., Kallevik, H., Sjoblom, J. 2001. Determination of saturate, aromatic, resin, and asphaltenic (SARA)
632 components in crude oils by means of infrared and near-infrared spectroscopy. *Energy Fuels*, v. 15, p. 1304-
633 1312

634 Aydin, A. 2000. Fractures, faults, and hydrocarbon entrapment, migration and flow. *Marine and Petroleum*
635 *Geology*, v. 17, no. 7, p. 797-814

636 Beaudoin, N. D., Huyghe, N., Bellahsen, O., Lacombe, L., Emmanuel, F., Mouthereau, & Ouahnnon, L.
637 2015. Fluid systems and fracture development during syn-depositional fold growth: An example from the Pico
638 del Aguila anticline, Sierras Exteriores, southern Pyrenees, Spain. *Journal of Structural Geology*, v. 70(C), p.
639 23–38, [doi:10.1016/j.jsg.2014.11.003](https://doi.org/10.1016/j.jsg.2014.11.003)

640 Bons, P.D., Arnold, J., Elburg, M.A., Kalda, J., Soesoo, A., & van Milligen, B. P. 2004. Melt extraction and
641 accumulation from partially molten rocks. *Lithos*, v. 78, p. 25–42, [doi:10.1016/j.lithos.2004.04.041](https://doi.org/10.1016/j.lithos.2004.04.041)

642 Bons, P.D., Elburg, M.A. and Gomez-Rivas, E. 2012. A review of the formation of tectonic veins and their
643 microstructures. *Journal of Structural Geology*, v. 43, p. 33-62

644 Burnham, A.K. 2017. *Global Chemical Kinetics of Fossil Fuels. How to Model Maturation and Pyrolysis:*
645 Amsterdam, Springer, 330 p

646 Childs, C., Sylta, Ø., Moriya, S., Morewood, N., Manzocchi, T., Walsh, J. J., & Hermanssen, D. 2009.
647 Calibrating fault seal using a hydrocarbon migration model of the Oseberg Syd area, Viking Graben. *Marine*
648 *and Petroleum Geology*, v. 26, Issue 6, p. 764-774. <https://doi.org/10.1016/j.marpetgeo.2008.05.004>

649 Comer, J.B. 2007. Reservoir Characteristics and Gas Production Potential of Woodford Shale in the Southern
650 Mid Continent. Woodford Gas Shale Conference, Indiana Geological Survey, <http://hdl.handle.net/2022/1826>

651 Davletbaev, A., Kovaleva, L., & Babadagli, T. 2011. Mathematical modeling and field application of heavy oil
652 recovery by Radio-Frequency Electromagnetic stimulation. *J. Pet. Sci. Eng.* v. 78 (3-4): p. 646-
653 653, <http://dx.doi.org/http://dx.doi.org/10.1016/j.petrol.2011.07.006>

654 Diabat, A. 2009. Structural and stress analysis in Amman area, based on fault slip data. The 9th Jordanian
655 Geological Conference and the 6th Geol. Symp. On Eastern Mediterranean Geology, Amman, 2- 5 April.

656 Diabat, A., & Masri, A. 2005. Orientation of the principal stresses along Zerqa–Ma'in Fault. *Mu'tah Lil- Buhuth*
657 *wad-Dirasat*, v.20, p. 57–71

658 Dyni, John R. 2006. Geology and resources of some world oil-shale deposits. Scientific Investigations Report
659 2005–5294. U.S. Department of the Interior. U.S. Geological Survey. Retrieved 2007-07-09

660 Eichhubl, P., Aydin, A. & Lore, J. 2001. Opening-mode fracture in siliceous mudstone at high homologous
661 temperature—effect of surface forces. *Geophysical Research Letter*, v. 28, p. 1299–1302

662 Eichhubl, P. & Aydin, A. 2003. Ductile opening-mode fracture by pore growth and coalescence during
663 combustion alteration of siliceous mudstone. *Journal of Structural Geology* v. 25, p. 121–34

664 Figueroa Pilz, F., Dowey, P.J., Fauchille, A.L., Courtois, L., Bay, B., Ma, L., Taylor, K.G., Mecklenburgh, J., &
665 Lee, P. D. 2017. Synchrotron tomographic quantification of strain and fracture during simulated thermal
666 maturation of an organic-rich shale, UK Kimmeridge Clay. *J. Geophys. Res. Solid Earth*, v. 122, p. 2553–2564,
667 [doi:10.1002/2016JB013874](https://doi.org/10.1002/2016JB013874)

668 Fink, R., Virgo, S., Arndt, M., Visser, W., Littke, R. & Urai, J.L. 2016. Solid bitumen in calcite veins from the
669 Natih Formation in the Oman Mountains: Multiple phases of petroleum migration in a changing stress field.

670 International Journal of Coal Geology, v. 157, p. 39-51, ISSN 0166-5162,
671 <https://doi.org/10.1016/j.coal.2015.07.012>

672 Gradstein, F.M., Ogg, J.G., Schmitz, M., & Ogg, G. 2012. Geologic Time Scale 2012. Elsevier B.V.,
673 Amsterdam

674 Gross, M.R., Fischer, M.P., Engelder, T. & Greenfield, R. J. 1995. Factors controlling joint spacing in
675 interbedded sedimentary rocks. Integrating numerical models with field observations from the Monterey
676 Formation, U.S.A., in M. S. Ameen, ed., Fractography. Fracture topography as a tool in fracture mechanics and
677 stress analysis: Geological Society Special Publication, v. 92, p. 215–233

678 Hakimi, M.H., Abdullah, W.H., Alqudah, M., Makeen, Y.M., & Mustapha, K.A. 2016. Organic geochemical
679 and petrographic characteristics of the oil shales in the Lajjun area, Central Jordan: origin of organic matter
680 input and preservation conditions. Fuel, v. 181, p. 34-45

681 Hakimi, M.H., Abdullah, W., Alqudah, M., Makeen, Y., Mustapha, K.A., & Hatem. B. 2018. Pyrolysis analyses
682 and bulk kinetic models of the Late Cretaceous oil shales in Jordan and their implications for early mature
683 sulphur-rich oil generation potential. Marine and Petroleum Geology, v. 91, p. 764-775,
684 <https://doi.org/10.1016/j.marpetgeo.2018.01.036>

685 Hamarneh, Y. 1998. Oil shale resources development in Jordan. Amman, Natural Resources Authority,
686 Hashemite Kingdom of Jordan, p 98

687 Hilgers, C., & Urai, J. L. 2002. Microstructural observations on natural syntectonic fibrous veins: implications
688 for the growth process. Tectonophysics, v. 352, p. 257-274

689 Hooker, J. N., Huggett, J. M., Cartwright, J., & Ali Hussein, M. 2017. Regional-scale development of opening-
690 mode calcite veins due to silica diagenesis. Geochim. Geophys. Geosyst., v. 18, p. 2580–2600,
691 [doi:10.1002/2017GC006888](https://doi.org/10.1002/2017GC006888)

692 Hooker, J. N., Abu-Mahfouz, I. S., Meng, Q., & Cartwright. J. 2018. Fractures in mudrocks. Advances in
693 constraining timing and understanding mechanisms: Journal of Structural Geology, in press,
694 <https://doi.org/10.1016/j.jsg.2018.04.020>

695 Huang W.Y. & Meinschein W.G. 1979. Sterols as ecological indicators. Geochim Cosmochim Acta, v. 43, p.
696 739–45

697 Huggett, J., Hooker, J. N. & Cartwright, J. 2017. Lithologic controls on diagenesis and diagenetic sequence in
698 the Al Hasa phosphorite, Muwaqqar chalk marl, and Um Rijam chert formations, Jordan: *Arabian J. Geosci.*, v.
699 10, p. 270, [doi:10.1007/s12517-017-3038-5](https://doi.org/10.1007/s12517-017-3038-5)

700 Huang W.Y., & Meinschein W.G. 1979. Sterols as ecological indicators. *Geochim Cosmochim Acta* 43:739–
701 745

702 Jaber, J. O., Probert, S. D., and Badr, O. 1997. Prospects for the exploitation of Jordanian oil shale. *Oil Shale*, v.
703 14(4), p. 565–578

704 Jochum, J., Friedrich, G., Leythaeuser, D., Littke, R., & Ropertz, B. 1995. Hydrocarbon-bearing fluid
705 inclusions in calcite-filled horizontal fractures from mature Posidonia Shale (Hils Syncline, NW Germany). *Ore*
706 *Geol. Rev.*, v. 9, p. 363–370

707 Jones, G., Fisher, O.J. & Knipe, R.J. 1998. Faulting, fault sealing and fluid flow in hydrocarbon reservoirs.
708 London Geological Society, Special Publication, v. 147, 319 p

709 Lüning, S., & Kuss, J. 2014. Petroleum geology of Jordan, in *Petroleum Systems of the Tethyan Region*, edited
710 by L. Marlow, C. Kendall, & L. Yose. AAPG Mem., v. 106, p. 217–239

711 Mandl, G., & Harkness, R.M. 1987. Hydrocarbon migration by hydraulic fracturing. In M. E. Jones, & R. M. F.
712 Preston, *Deformation of sediments and sedimentary rocks*. Geological Society Special Publication, v. 29, pp.
713 39-53

714 März, C., Wagner, T., Aqleh, S., Al-Alaween, M., van den Boorn, S., Podlaha, O.G., Kolonic, S., Poulton,
715 S.W., Schnetger, B., & Brumsack, H.J., 2016, Repeated enrichment of trace metals and organic carbon on an
716 Eocene high-energy shelf caused by anoxia and reworking. *Geology*, v. 44 (12), pp.1011–1014, doi:
717 <https://doi.org/10.1130/G38412.1>

718 McDermott, C. I., Edlmann, K. & Haszeldine, R.S., 2013, Predicting hydraulic tensile fracture spacing in strata-
719 bound systems. *International Journal of Rock Mechanics and Mining Sciences*, v. 63, p. 39-49,
720 doi.org/10.1016/j.ijrmms.2013.06.004

721 Mello, M.R., Telnaes, N., Gaglianone, P.C., Chicarelli, M. I., Brassell, S.C., & Maxwell, J.R. 1988. Organic
722 geochemical characterisation of depositional palaeoenvironments of source rocks and oils in Brazilian marginal
723 basins. *Organic Geochemistry*, v. 13, p. 31–45

724 Michels, R., Landais, P., Philp, R.P., & Torkelson, B.E. 1994. Effects of pressure on organic matter maturation
 725 during confined pyrolysis of Woodford kerogen. *Energy Fuel*, v. 8 (3), p. 741–754

726 Mueller, E., & Philp, E. 1998. Extraction of high molecular weight hydrocarbons from source rocks: an
 727 example from the Green River Formation, Uinta Basin, Utah. *Organic Geochemistry*, v. 28, Issues 9–10, p. 625-
 728 631, [https://doi.org/10.1016/S0146-6380\(98\)00031-X](https://doi.org/10.1016/S0146-6380(98)00031-X)

729 Meng, Q., Hooker, J. N. & Cartwright, J. 2017. Early overpressuring in organic-rich shales during burial.
 730 Evidence from fibrous calcite veins in the Lower Jurassic Shales-with-Beef Member in the Wessex Basin, UK:
 731 *J. Geol. Soc.*, [doi:10.1144/jgs2016-146](https://doi.org/10.1144/jgs2016-146)

732 Nelson, R.A. 1985. *Geological Analysis of Naturally Fractured Reservoirs: Houston TX*, Gulf Publishing, 332
 733 p.

734 Olson, J.E., Laubach, S.E. & Lander, R.H. 2009. Natural fracture characterization in tight gas sandstones:
 735 integrating mechanics and diagenesis. *AAPG Bull.* v. 93, p. 1535-1549, [doi: 10.1306/08110909100](https://doi.org/10.1306/08110909100)

736 Parnell, J., Robinson, N. & Brassell, S. 1991. Discrimination of bitumen sources in Precambrian and Lower
 737 Palaeozoic rocks, southern U.K., by gas chromatography–mass spectrometry. *Chemical Geology*, v. 90, p. 1–14

738 Parnell, J., Geng, A., Fu, J., & Sheng, G. 1994. Geology and geochemistry of bitumen vein deposits at Ghost
 739 City, Junggar Basin, northwest China. *Geol. Mag.* v. 131, p. 181-190

740 Parnell, J., & Carey, P. F. 1995. Emplacement of bitumen (asphaltite) veins in the Neuquen Basin, Argentina.
 741 *AAPG Bulletin*, v. 79 (12), p. 1798-1816

742 Parnell, J., Carey, P. & Monson, B. 1998. Timing and temperature of decollement on hydrocarbon source rock
 743 beds in cyclic lacustrine successions. *Palaeogeography, Palaeoclimatology, Palaeoecology*, v. 140, p. 121–134

744 Parnell, J., Baron, M., Mann, P., & Carey, P. 2003. Oil migration and bitumen formation in a hydrothermal
 745 system, Cuba. *Journal of Geochemical Exploration*, v. 78–79, p. 409-415, [https://doi.org/10.1016/S0375-](https://doi.org/10.1016/S0375-6742(03)00018-9)
 746 [6742\(03\)00018-9](https://doi.org/10.1016/S0375-6742(03)00018-9)

747 Parnell, J., Baba, M., Bowden, S., & Muirhead, D. 2017a. Subsurface biodegradation of crude oil in a fractured
 748 basement reservoir, Shropshire, UK. *Journal of the Geological Society*, v. 174, p. 655-
 749 666, <https://doi.org/10.1144/jgs2016-129>

750 Parnell, J., Baba, M., & Bowden, S. 2017b. Emplacement and biodegradation of oil in fractured basement: The
 751 'coal' deposit in Moinian gneiss at Castle Leod, Ross-shire. *Earth and Environmental Science Transactions of*
 752 *the Royal Society of Edinburgh*, 107(1), 23-32. [doi:10.1017/S1755691017000056](https://doi.org/10.1017/S1755691017000056)

753 Passchier, S. 2000. Soft-sediment deformation features in core from CRP-2/2A, Victoria Land Basin,
 754 Antarctica, *Terra Antarctica*, Bremerhaven, PANGAEA, v. 7 (3), p. 401-412

755 Pathak, V., Babadagli, T., & Edmunds, N. 2013. Experimental Investigation of Bitumen Recovery from
 756 Fractured Carbonates Using Hot Solvents. *Society of Petroleum Engineers*, v. 52, [doi:10.2118/159439-PA](https://doi.org/10.2118/159439-PA)

757 Pepper, A. 2017. Definition, Modes of Occurrence and Pitfalls in Understanding the Term 'Bitumen' in
 758 Conventional and Unconventional Petroleum Systems. paper presented to AAPG Annual Convention and
 759 Exhibition, Houston, Texas.

760 <http://www.searchanddiscovery.com/abstracts/html/2017/90291ace/abstracts/2613048.html>.

761 Peters, K.E., & Moldowan, J. 1993. *The biomarker Guide. Interpreting molecular fossils in petroleum and*
 762 *ancient sediments*, Prentice hall, Englewood cliffs, NJ, 363 p

763 Peters, K.E., Moldowan, J.M., McCaffrey, M.A., & Fago, F.J. 1996. Selective biodegradation of extended
 764 hopanes to 25-norhopanes in petroleum reservoirs. *Insights from molecular mechanics; Organic*
 765 *Geochemistry*, v. 24, p. 765–783

766 Peters, K.E., Walters, C. & Moldowan, J. 2005. *The Biomarker Guide. Biomarkers and isotopes in petroleum*
 767 *systems and Earth history*: New York, Cambridge university press, v. 2, 2nd edition.

768 Powell, J.1989. *Stratigraphy and Sedimentation of the Phanerozoic Rocks in Central and South Jordan; Part B,*
 769 *Kurnub, Ajlun and Belqa Groups. Geol. Mapping Div. Bull. 11A*, Natural Resources Authority, Amman

770 Powell, J., & Moh'd, B. 2011. Evolution of Cretaceous to Eocene alluvial and carbonate platform sequences in
 771 central and south Jordan. *GeoArabia*, v. 16 (4), p. 29-82

772 Prajapati, N., Selzer, M., Nestler, B., Busch, B., and Hilgers. C., 2018, Modeling fracture cementation processes
 773 in calcite limestone: a phase-field study: *Geotherm Energy*. v. 6: 7. <https://doi.org/10.1186/s40517-018-0093-4>

774 Priest, S. D., & Hudson, J. A., 1981, Estimation of discontinuity spacing and trace length using scanline
775 surveys: International Journal of Rock Mechanics and Mining Sciences and Geomechanics Abstracts, v. 18, p.
776 183–197.

777 Priest, S. D., 1993, Discontinuity analysis for rock engineering: London, Chapman & Hall, 473 p. Ryder, R. T.,
778 Hackley, P. C. Trippi, M. H., & Alimi. H., 2013, Evaluation of thermal maturity in the low maturity Devonian
779 shales of the northern Appalachian Basin: AAPG Search and Discovery Article 10477. Parts 1 (67 p.) and 2
780 (177 p.) http://www.searchanddiscovery.com/documents/2013/10477ryder/ndx_ryder.pdf

781 Secor, D.T. 1965. Role of fluid pressure in jointing: American Journal of Science, v. 263, p. 633–646.

782 Segev, A., Lyakhovsky, V., & Weinberger, R. 2014. Continental transform–rift interaction adjacent to a
783 continental margin: The Levant case study: Earth-Science Reviews, v. 139, p. 83-103,
784 <https://doi.org/10.1016/j.earscirev.2014.08.015>

785 Seifert W. K., & Moldowan J. M., 1981, Paleoconstruction by biological markers: Geochim Cosmochim Acta;
786 v. 45, no. 6, p. 783–794, [doi: 10.1016/0016-7037\(81\)90108-3](https://doi.org/10.1016/0016-7037(81)90108-3)

787 Selby, D. & Creaser, R. A. 2005. Direct radiometric dating of hydrocarbon deposits using rhenium-osmium
788 isotopes: Science, v. 308, p. 1293 – 1295, [doi: 10.1126/science.1111081](https://doi.org/10.1126/science.1111081)

789 Sinninghe-Damste, J., Kenig, F., Koopmans, M., Koster, J., Schouten, S., Hayes, J., & DeLeeuw, J., 1995,
790 Evidence for gammacerane as an indicator of water column stratification: Geochimica et Cosmochimica Acta,
791 v. 59, p.1895-1900.

792 Sokol E. V., Kozmenko O. A., Khoury H. N., Kokh S. N., Novikova S. A., Nefedov A. A., Sokol I. A., &
793 Zaikin P. 2017. Calcareous sediments of the Muwaqqar chalk marl formation, Jordan: mineralogical and
794 geochemical evidences for Zn and Cd enrichment: Gondwana Res, v. 46, p. 204-
795 226, <https://doi.org/10.1016/j.gr.2017.03.008>

796 Stern, R. J. & Johnson, P. 2010. Continental lithosphere of the Arabian Plate: A geologic, petrologic, and
797 geophysical synthesis: Earth Science Reviews, v. 101, p. 29-67

798 Teufel, L. W., & Clark, J. A. 1984. Hydraulic fracture propagation in layered rocks: experimental studies of
799 fracture containment: Soc Petrol Eng J, v. 24, p. 19–32

800 Tissot B. P., & Welte D. H. 1984. Diagenesis, Catagenesis and Metagenesis of Organic Matter: Petroleum
 801 Formation and Occurrence., Berlin, Heidelberg, Springer, p. 69-73, [https://doi.org/10.1007/978-3-642-96446-](https://doi.org/10.1007/978-3-642-96446-6_6)
 802 [6_6](https://doi.org/10.1007/978-3-642-96446-6_6)

803 Verbeek, E. R., & Grout, M. A., 1992, Hydrocarbon and mineral resources of the Uinta Basin, Utah and
 804 Colorado ed T D Fouch, V F Nuccio et al (Salt Lake: Utah Geological Association Guidebook 20) Structural
 805 evolution of gilsonite dikes, eastern Uinta Basin, Utah, p. 237-255

806 Volkman J. K.. 1986. A review of sterol biomarkers for marine and terrigenous organic matter: Org Geochem,
 807 v. 9, p. 83–9

808 Wang, G., Wang, T. G., Han, K., Wang, L. & Chi, S. 2015. Recognition of a novel Precambrian petroleum
 809 system based on isotopic and biomarker evidence in the Yangtze platform, South China: Marine and Petroleum
 810 Geology, v. 68, p. 414–426. doi.org/10.1016/j.marpetgeo.2015.09.003

811 Wang H., Yao Y., Liu D., Pan , Z., Yang, Y., & Cai Y. 2016. Fault-sealing capability and its impact on coalbed
 812 methane distribution in the Zhengzhuang field, southern Qinshui Basin, North China: Journal of Natural Gas
 813 Science and Engineering, v. 28, p. 613-625. [doi: 10.1016/j.jngse.2015.12.036](https://doi.org/10.1016/j.jngse.2015.12.036).

814 Wilhelms, A., Larter, S. R., Head, I., Farrimond, P., di-Primio, R. & Zwach, C. 2001. Biodegradation of oil in
 815 uplifted basins prevented by deep-burial sterilization: Nature, v. 411, p. 1034–1037

816 Yassini, I. 1979. Maastrichtian-Lower Eocene biostratigraphy and the planktonic foraminiferal biozonation in
 817 Jordan: Rev. Esp. Micropaleontol. 11, 5e57

818 Zeeb, C., Gomez-Rivas, E., Bons, P. D., & Blum, P. 2013. Evaluation of sampling methods for fracture network
 819 characterization using outcrops: AAPG Bull., v. 97, p. 1545-1566, [doi:10.1306/02131312042](https://doi.org/10.1306/02131312042)

820 Zhang, J., Z. Jiang, X. Jiang, S. Wang, C. Liang, & M. Wu. 2016. Oil generation induces sparry calcite
 821 formation in lacustrine mudrock, Eocene of east China: Mar. Pet. Geol., v. 71, p. 344–359,
 822 doi.org/10.1016/j.marpetgeo.2016.01.007

823 **Figure captions**

824 **Fig. 1. (a)** Structural map of Jordan, showing the location of the studied fifteen cores and the outcrop in
 825 Central and South Jordan, and the main structural elements in the region (Modified after Diabat & Masri
 826 2005). Numbers from 1 to 15 represent the studied cores (C1-C15). **(b)** The stratigraphy of the Belqa
 827 Group in outcrop and subsurface. Blue shaded part represents the studied succession (modified after Ali

828 Hussein *et al.* 2014b). (c) and (d) Schematic E-W and N-S structural cross sections across the area of
829 Jordan (modified after Lüning & Kuss 2014 and Natural Resources Authority of Jordan (NRA 2001).

830 **Fig. 2.** (a) A columnar section showing the lithology of the studied cored intervals. (b) A representative
831 trend (from core 10) of vertical frequency and distribution of all fractures and bitumen-bearing fractures
832 against the three lithological units. Zoomed in area demonstrates the relationship between fracture
833 intensity and the TOC and TS of the lower unit. Red-shaded rectangles show low fracture intensity
834 correlate with low TOC and TS values. Green-shaded rectangles show high fracture intensity correlates
835 with high TOC and TS values. (c). Schematic drawing showing the age difference of the JOS in different
836 cores from central west, central east and south Jordan (modified after Alqudah *et al.* 2015). C5 in this
837 study is equivalent to OS22, C8 to OS28 and C13 to OS1 in the Alqudah *et al.* (2015) study (see
838 supplementary Table for more information). Absolute ages after Gradstein *et al.* (2012).

839 **Fig. 3.** (a) Schematic burial history curve of the JOS in the Harrana area (CW) and (b) in the Azraq area
840 (CE).

841 **Fig. 4.** Plots showing (a) the frequency of all opening-mode fractures in the core and (b) The frequency
842 of veins (planar and folded veins).

843 **Fig. 5.** Slabbed core images of different bitumen-bearing fractures. B, Bitumen; BCV, Bitumen-Bearing
844 Calcite Vein; CV, Calcite Vein; BV, Bitumen Vein; SV, Silica Vein; FCV, Folded Calcite Vein, BMF,
845 Bitumen Microfracture; S. Mudstone, Silicified mudstone. (a) BCV propagates across chert nodule,
846 silicified mudstone, and organic-rich mudstone. Note the deflection of vein when the bed lithology
847 changes (blue arrows). (b) BVs confined to chert beds and carbonate concretion. Note the low-organic
848 matter zone in the mudstone bed underlying the chert bed (yellow dotted), indicating that bitumen has
849 escaped towards the chert bed (white-dashed arrow). (c) Bitumen-bearing calcite veins confined to chert
850 beds/lenses; demonstrating the role of mechanical stratigraphy in fracturing. (d) Bitumen vein
851 propagates through three different types of lithologies (mudstone, chert and carbonate concretion). Note
852 the increase in aperture size of the vein in the chert and carbonate concretions. (e) BV open towards the

853 chert concretion. Note the low-organic matter zone in the mudstone bed overlying the chert concretion
854 (yellow dotted); indicates bitumen migration towards the centre of the chert concretion (white-dashed
855 arrow). (f) Two fracture networks of horizontal and vertical SVs and BVs. BVs crosscut SVs (Blue
856 arrow). (g) Mosaic brecciation in the organic-rich mudstone.

857 **Fig. 6.** Core and field photographs of different bitumen-bearing veins. BCV, Bitumen-bearing Calcite
858 Vein; BV, Bitumen Vein; SV, Silica Vein; FCV, Folded Calcite Vein; S. Mudstone, Silicified mudstone.
859 (a) SVs and BVs in organic-rich mudstone. (b) Schematic drawing of (a). Note the crosscutting
860 relationship between silica veins and bitumen veins (blue arrows). (c) Field photograph of vertical BVs
861 confined to the oil shale bed at the El-Lajjun quarry. (d) Bitumen in veins and pores (vugs) in silicified
862 limestone beds in the lower unit of core C8. Yellow diamonds show the maximum aperture size of the
863 bitumen vein. (e) Bitumen vein propagates in mudstone and chert beds. Note the branching of the
864 bitumen vein in the mudstone bed (yellow arrow). (f) Horizontal BCV crosscut folded calcite veins in
865 organic-rich mudstone. (g) Schematic drawing of (f). Note the crosscutting relationships between the
866 horizontal bitumen-bearing vein and folded veins (blue arrows).

867 **Fig. 7.** Micrographs of different bitumen-bearing fractures. BCV, Bitumen-bearing Calcite Vein; B,
868 Bitumen; BP, Bitumen-bearing pore, BMV, Bitumen Micro-Vein; BV, Bitumen Vein. (a) BCV shows
869 crack-seal texture. Note the bitumen inclusions within calcite cement. (b) Schematic drawing of (a). (c)
870 BSE image shows sub-horizontal microfractures, pores and microfossils filled with bitumen. Note
871 Microfracturing of grains. (d) EDS map of the bitumen microveins shown in (c), showing the Carbon
872 content in the bitumen microfractures and matrix in the lower unit of core. (e) Core photograph showing
873 BVs in carbonate concretions hosted by organic-rich mudstone. (f) Micrograph of the inset in (e)
874 showing the direction of bitumen migration inside both BV (white-dashed arrow) and BMV from the
875 organic-rich mudstone bed towards the carbonate concretion. (g) Mosaic brecciation of mudstone by
876 bitumen overpressure.

877 **Fig. 8.** Plot of Hydrogen index (HI) versus Tmax, showing maturity and kerogen quality of the Late
878 Cretaceous-Eocene oil shale samples.

879 **Fig. 9.** Examples of representative m/z 191 and m/z 217 fragmentograms showing the distribution of
880 terpanes and steranes, respectively, in studied matrix and fracture bitumen samples. Note the similarity
881 between the fracture (FB) and matrix bitumen (MB).

882 **Fig. 10.** Ternary diagram showing the distribution of C27, C28 and C29 $\alpha\alpha\alpha$ -R steranes in the fracture
883 and matrix bitumen samples. Depositional environments after Huang & Meinschein 1979.

884 **Fig. 11.** Plots of the hopane and sterane biomarkers ratios. a. 22S/(22S+22R) C31 Hopanes against
885 20S/(20S+20R) C28 Steranes. b: Gammacerane:C30 against C27 $\alpha\alpha\alpha$ R.

886 **Fig. 12.** Bitumen mobilization due to mechanical compaction (**a-d**). (**a**) Organic particle at shallow
887 burial. (**b**) Mechanical compaction and water removal. (**c**) It becomes mechanically weak-loading and
888 extrudes bituminized OM. Occurs preferentially in OM with early generation kinetics and high HI. (**d**)
889 Saturation of the matrix followed by short-distance migration, creating fractures (modified after Pepper
890 2017).

891 **Fig. 13.** Paragenetic sequence of the fracture cements (modified after Hooker *et al.* 2017).

Type of Bitumen-bearing fracture/ vugs	Carbonate concretion	Chert Concretion/Bed	Silicified Limestone	Silicified Mudstone	Marl	Organic-rich Mudstone	Dolomite	Re-Sedimented Bed
BV	H	H	H	H	M	H	H	H
BCV	M	M	H	H	M	M	M	-
BSV	L	H	M	H	-	-	-	-
Bitumen Vugs	M	H	H	M	-	-	H	H

Table 1. *Relative distribution of bitumen-bearing fractures and vugs (High: H, Moderate: M, Low: L)*

Sample	Sample Type	TOC (wt%)	TS (wt%)	S1 (mg/g rock)	S2 (mg/g rock)	T _{max} (°C)	HI (mg HC/g TOC)	OI (mg CO ₂ /g TOC)	PI
1	Core	19.5	2.8	2.7	148.2	402.0	762.0	17.4	0.02
2	Core	15.7	4.8	1.7	105.3	413.0	672.8	19.3	0.02
3	Core	16.9	3.8	2.0	115.0	420.0	680.5	15.3	0.02
4	Core	14.9	5.2	1.8	131.2	415.0	880.2	8.5	0.06
5	Core	15.9	4.5	2.5	112.4	416.0	705.7	11.4	0.02
6	Core	30.0	8.3	6.7	175.0	404.0	583.3	27.0	0.04
7	Core	14.1	2.3	0.9	104.5	416.0	743.5	9.3	0.01
8	Core	17.9	4.3	5.5	115.9	424.0	647.5	14.2	0.05
9	Core	20.2	4.3	1.9	130.0	395.0	642.9	12.9	0.04
10	Core	13.9	6.5	2.0	97.8	404.0	703.6	15.2	0.02
11	Core	14.9	3.7	1.4	100.1	405.0	670.7	12.0	0.01
12	Outcrop	21.3	3.9	4.6	132.3	416.0	621.1	13.7	0.03
13	Core	6.1	1.5	0.5	45.0	403.0	734.1	18.0	0.01
14	Core	12.4	2.8	1.8	90.3	409.0	726.6	13.0	0.02
15	Core	17.4	3.8	3.8	119.4	407.0	688.1	12.7	0.03
16	Core	11.7	4.7	2.5	90.4	389.2	771.9	14.3	0.06

Table 2. *Bulk organic geochemical properties of the JOS matrix in the lower unit of the studied succession*

Sample	Hopanes Data			Steranes Data							
	Gammacerane:C30	C29:C30	22S/(22S+22R) C31 Hopanes	%C27 $\alpha\alpha\alpha$ R	%C28 $\alpha\alpha\alpha$ R	%C29 $\alpha\alpha\alpha$ R	C27:C28	C27:C29	C28:C29	$\alpha\beta\beta/(\alpha\beta\beta+\alpha\alpha\alpha)$ C28 Steranes	20S/(20S+20R) C28 Steranes
FB1	0.48	0.52	0.21	52	25	23	2.10	2.32	1.11	0.59	0.30
FB2	0.37	0.39	0.25	55	21	24	2.61	2.24	0.86	0.59	0.25
FB3	0.79	0.60	0.53	48	26	26	1.85	1.85	1.00	0.51	0.52
FB4	0.79	0.53	0.54	47	27	25	1.72	1.85	1.07	0.49	0.51
FB5	0.46	0.27	0.53	58	20	22	2.88	2.58	0.89	0.49	0.47
FB6	0.47	0.38	0.56	52	23	25	2.23	2.04	0.92	0.55	0.42
FB7	0.45	0.38	0.56	48	24	27	2.00	1.77	0.88	0.54	0.39
FB8	0.87	0.35	0.55	54	20	26	2.67	2.09	0.78	0.63	0.40
FB9	0.90	0.33	0.60	57	20	23	2.82	2.53	0.89	0.63	0.43
FB10	0.93	0.28	0.55	57	18	25	3.21	2.25	0.70	0.65	0.42
FB11	0.89	0.36	0.60	58	21	22	2.81	2.65	0.94	0.66	0.43
FB12	0.44	0.44	0.28	53	21	26	2.58	2.04	0.79	0.50	0.24
MB1	0.57	0.43	0.19	53	23	24	2.33	2.23	0.95	0.59	0.28
MB2	0.38	0.27	0.22	53	20	27	2.67	2.00	0.75	0.53	0.25
MB3	0.77	0.54	0.55	49	23	27	2.11	1.82	0.86	0.41	0.51
MB4	0.76	0.49	0.56	47	24	29	1.96	1.63	0.83	0.51	0.52
MB5	0.40	0.38	0.56	55	22	24	2.53	2.29	0.90	0.59	0.44
MB6	0.38	0.52	0.55	56	20	24	2.72	2.33	0.86	0.57	0.44
MB7	0.34	0.53	0.57	56	21	23	2.72	2.45	0.90	0.57	0.38
MB8	0.84	0.28	0.57	55	21	24	2.67	2.29	0.86	0.64	0.42
MB9	0.88	0.29	0.58	55	20	25	2.67	2.18	0.82	0.62	0.45
MB10	0.91	0.33	0.56	54	20	26	2.67	2.09	0.78	0.63	0.42
MB11	0.83	0.36	0.56	52	23	24	2.23	2.13	0.96	0.60	0.45
MB12	0.45	0.41	0.27	51	16	30	2.58	1.69	0.66	0.52	0.21

Table 3. Biomarker data extracted from m/z 191 and m/z 217 fragmentograms of the analysed matrix and fracture samples

Figure 1

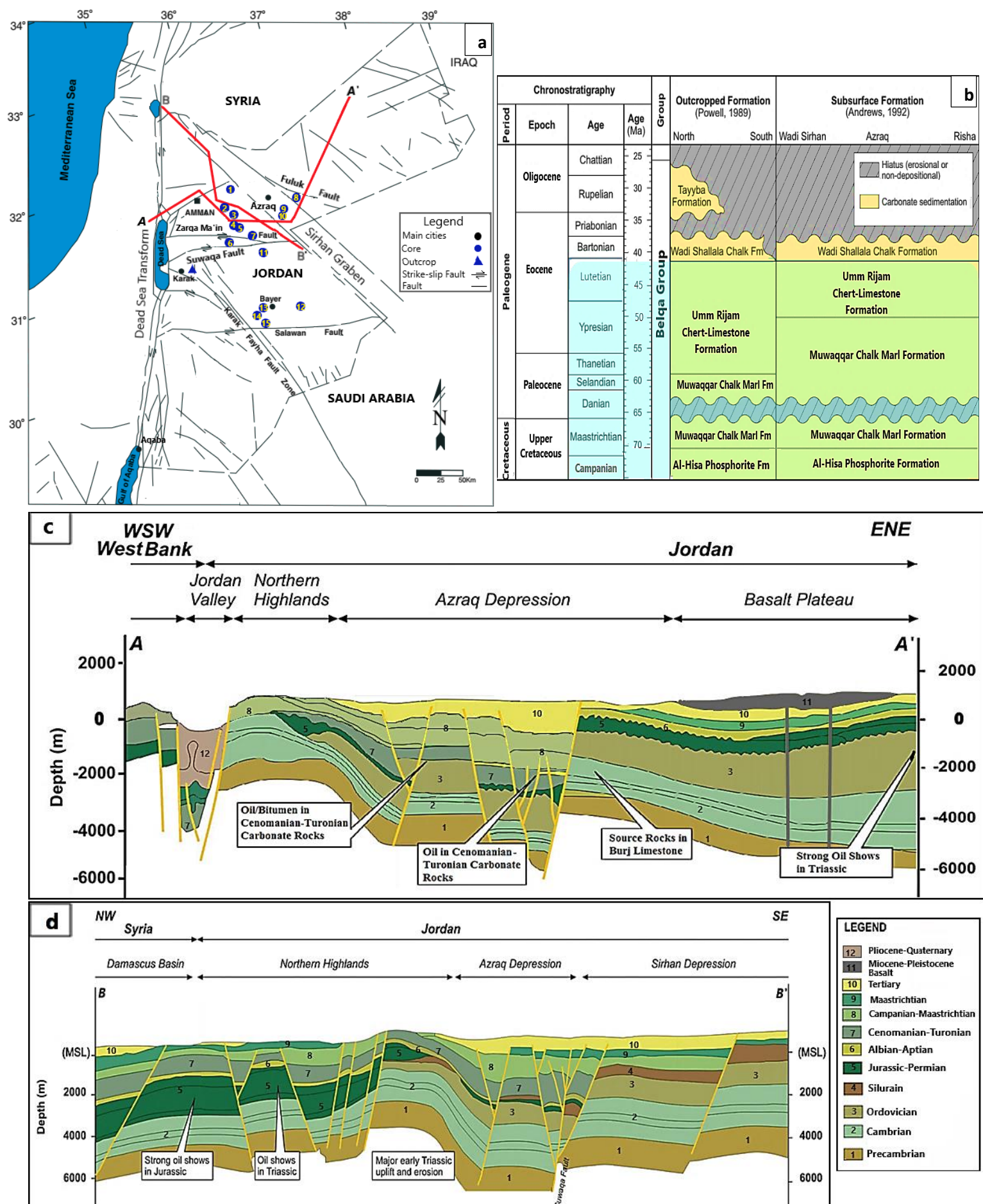


Figure 2

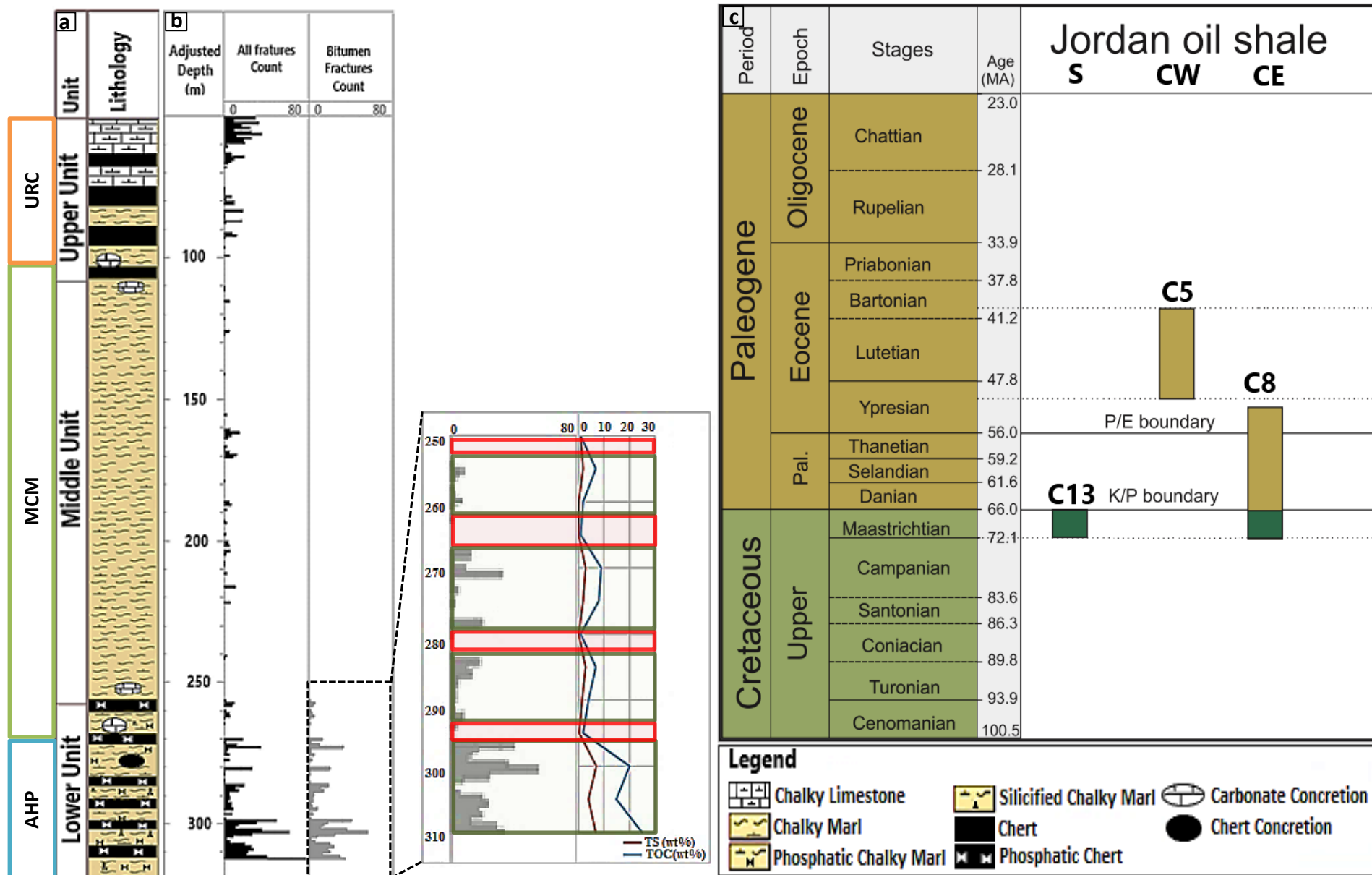


Figure 3

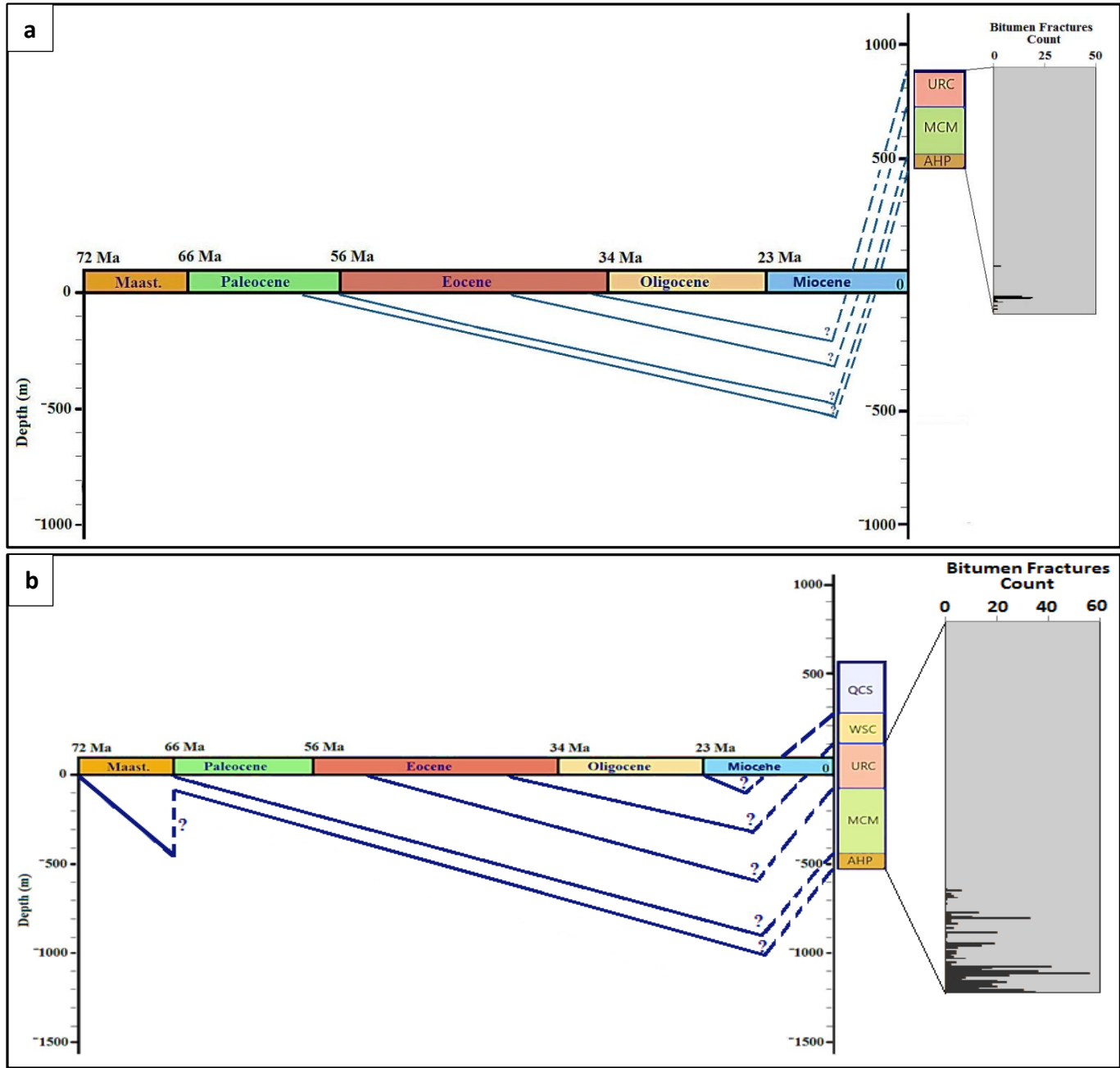


Figure 4

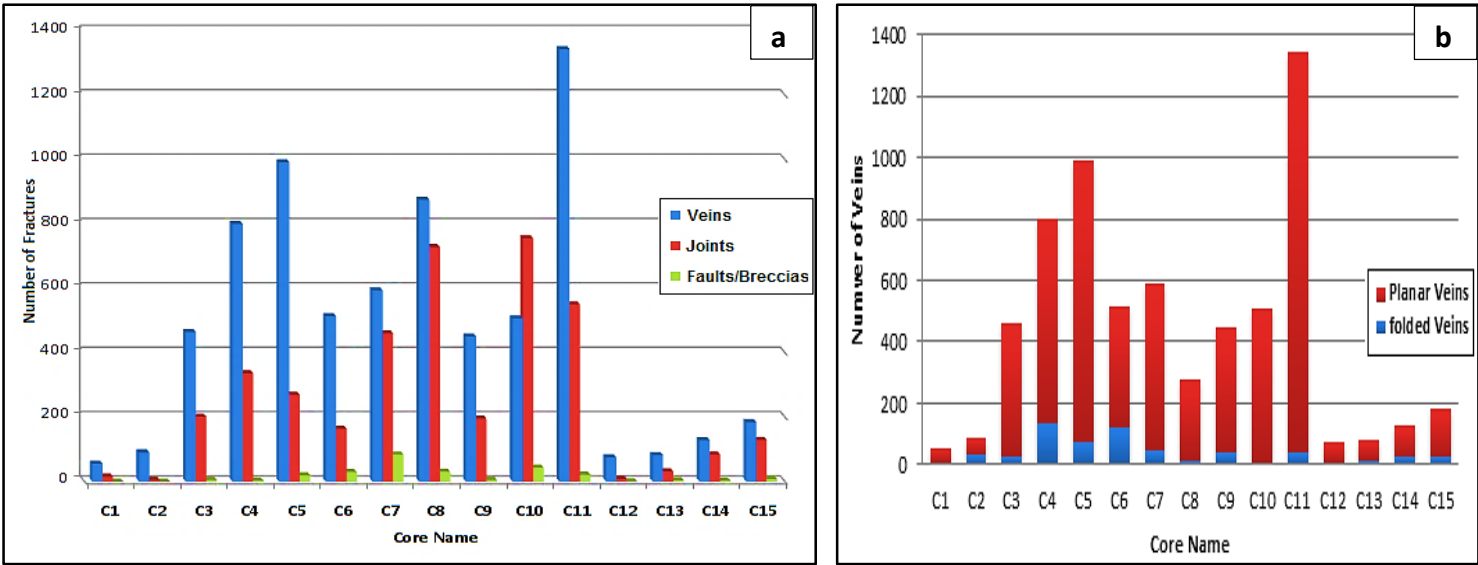


Figure 5

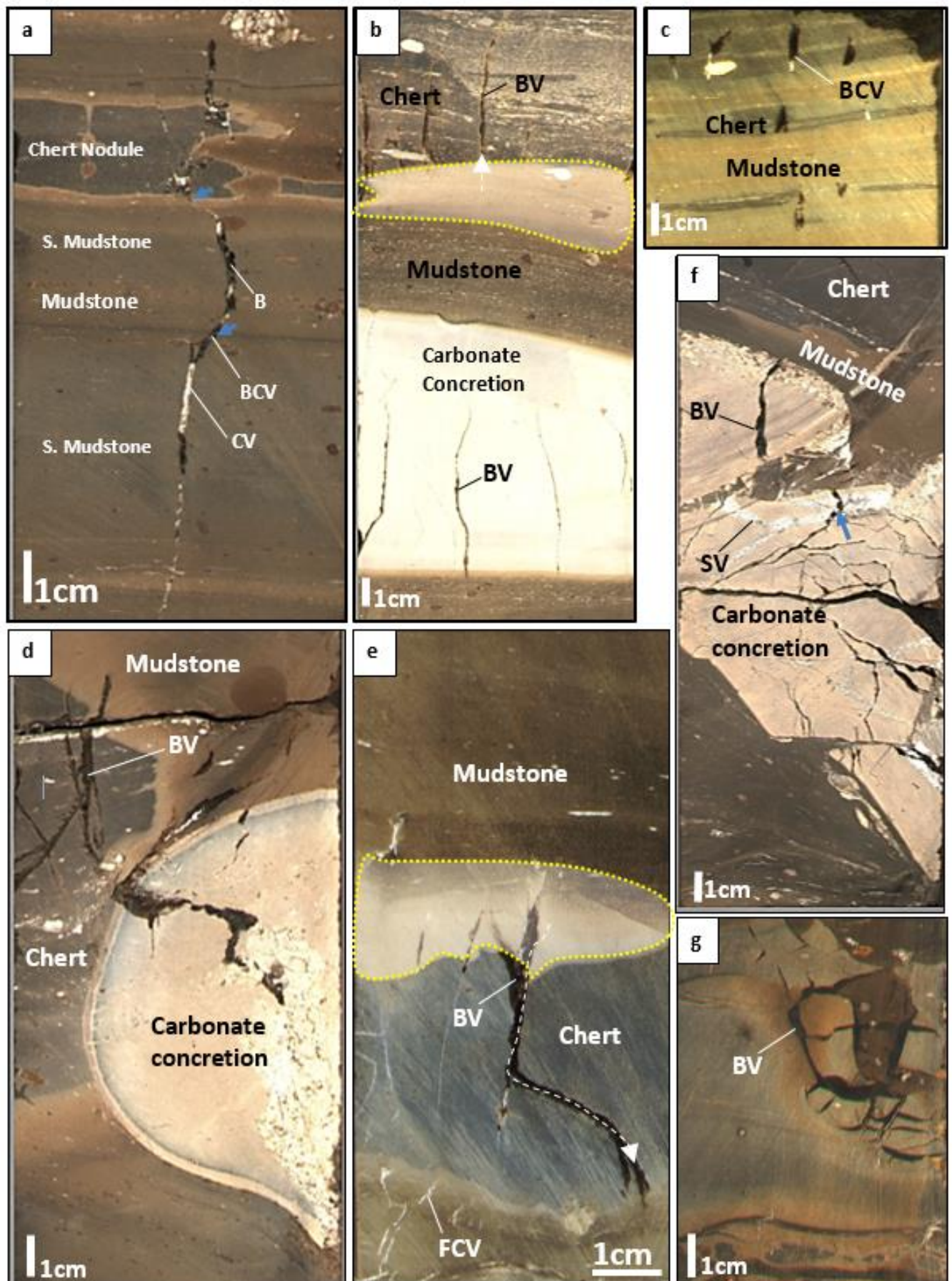


Figure 6

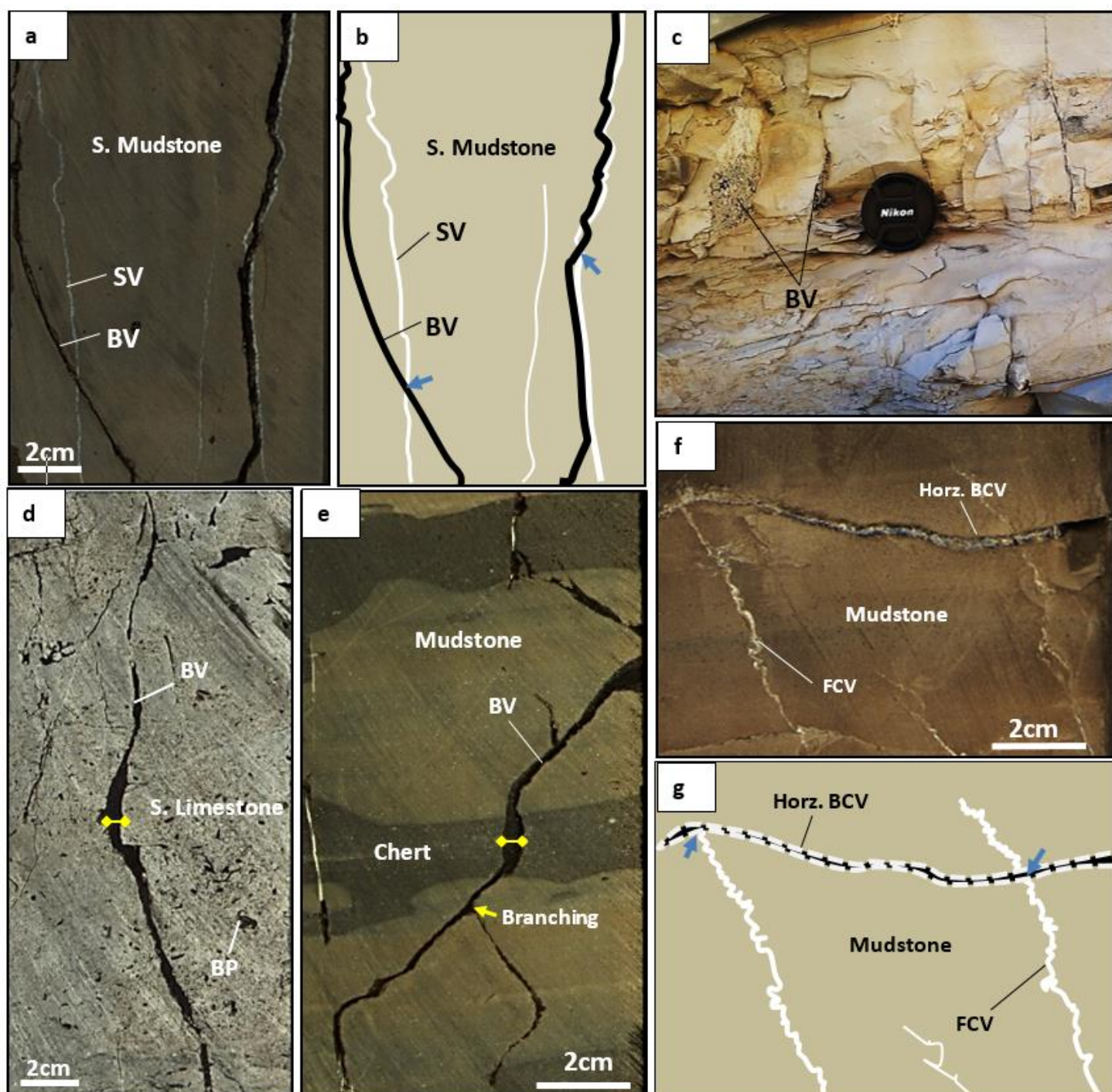


Figure 7

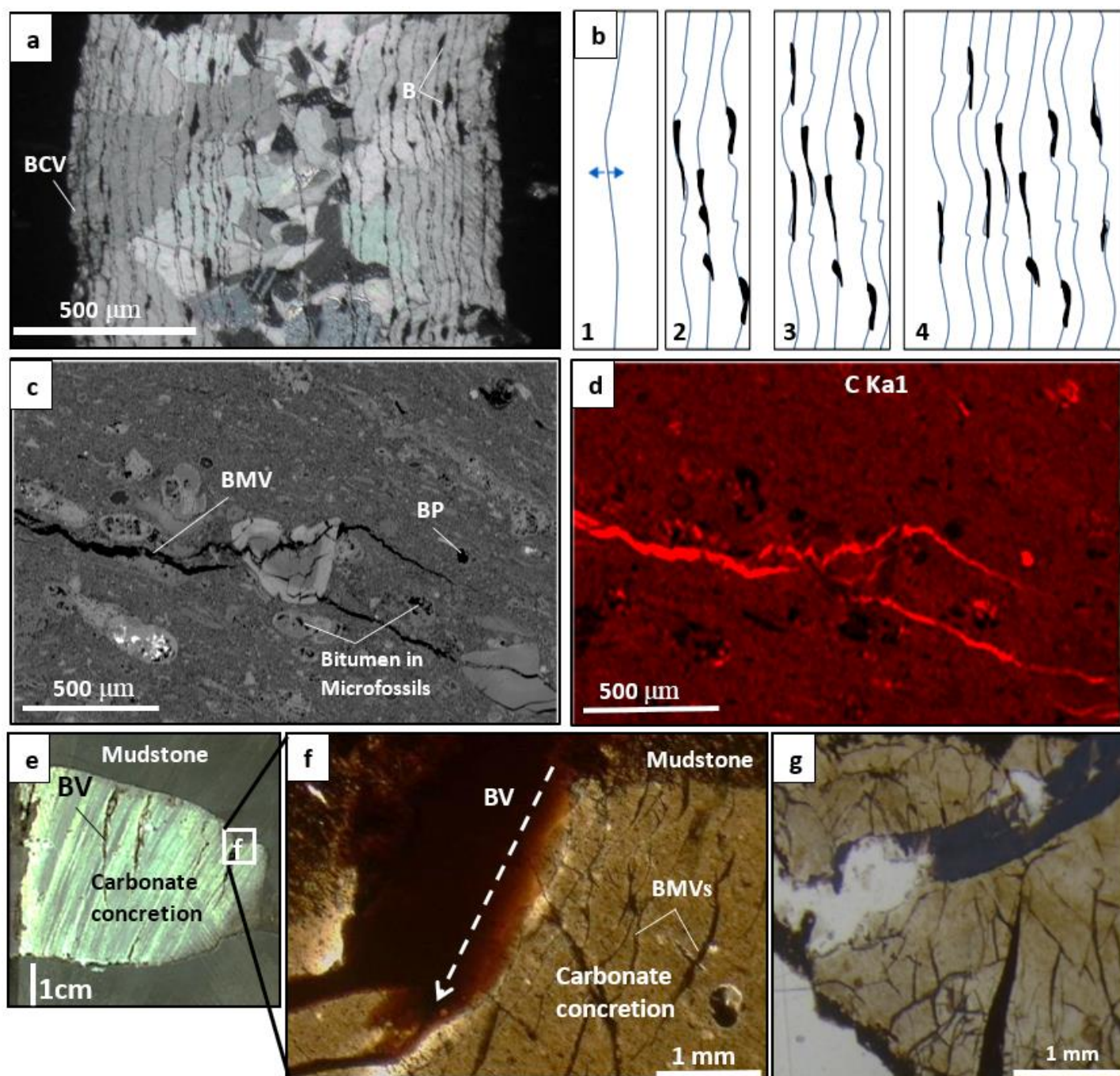


Figure 8

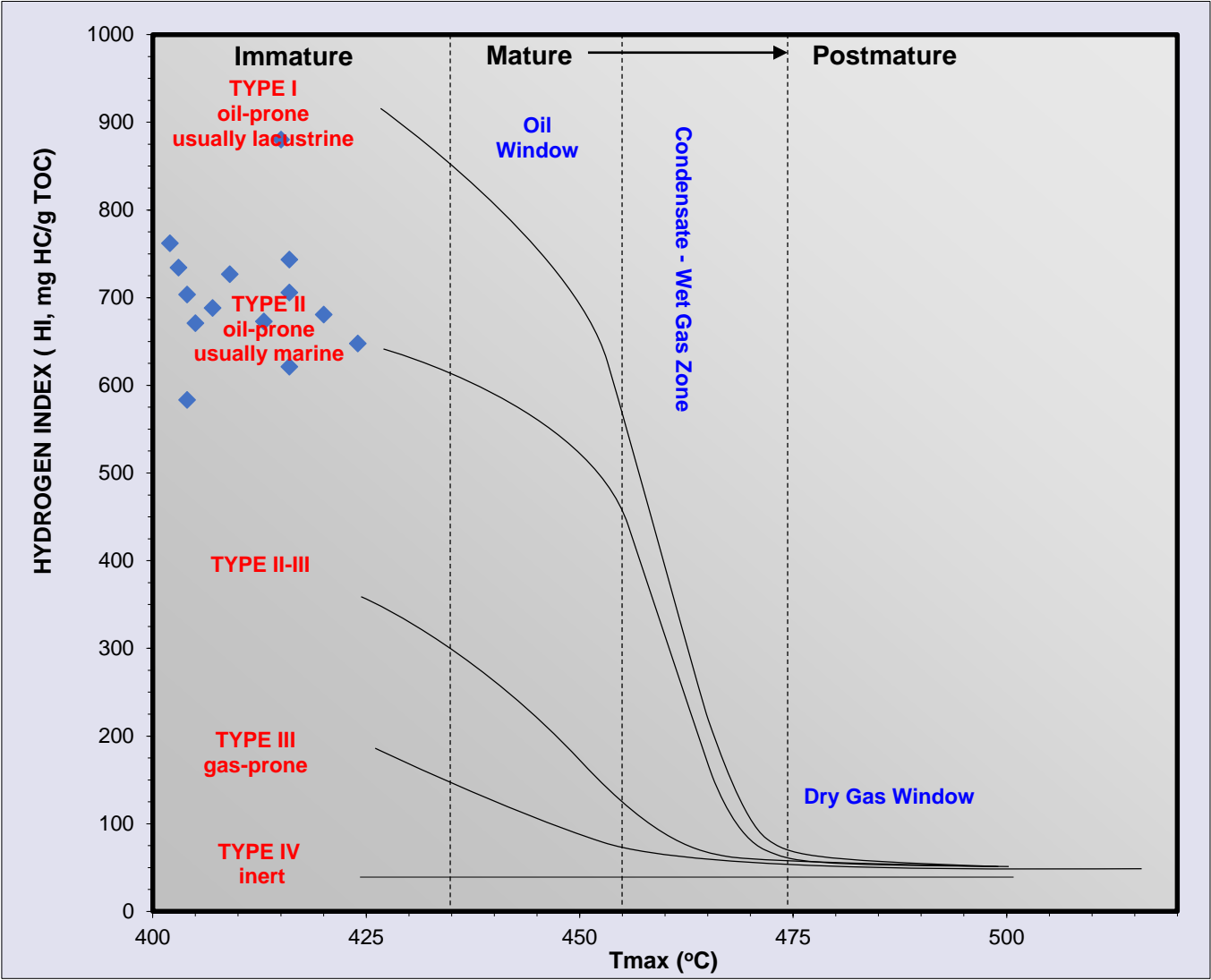


Figure 9

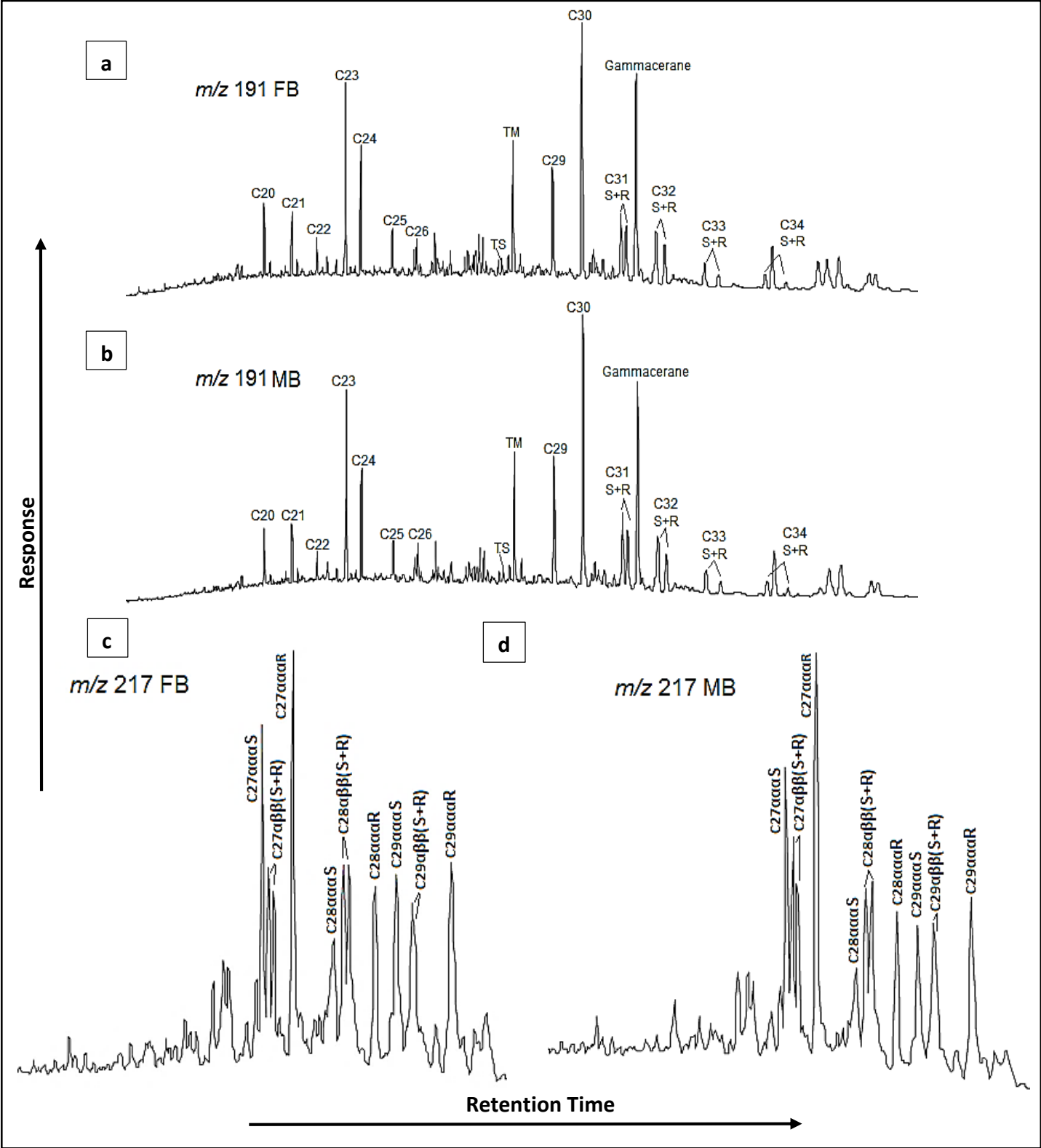


Figure 10

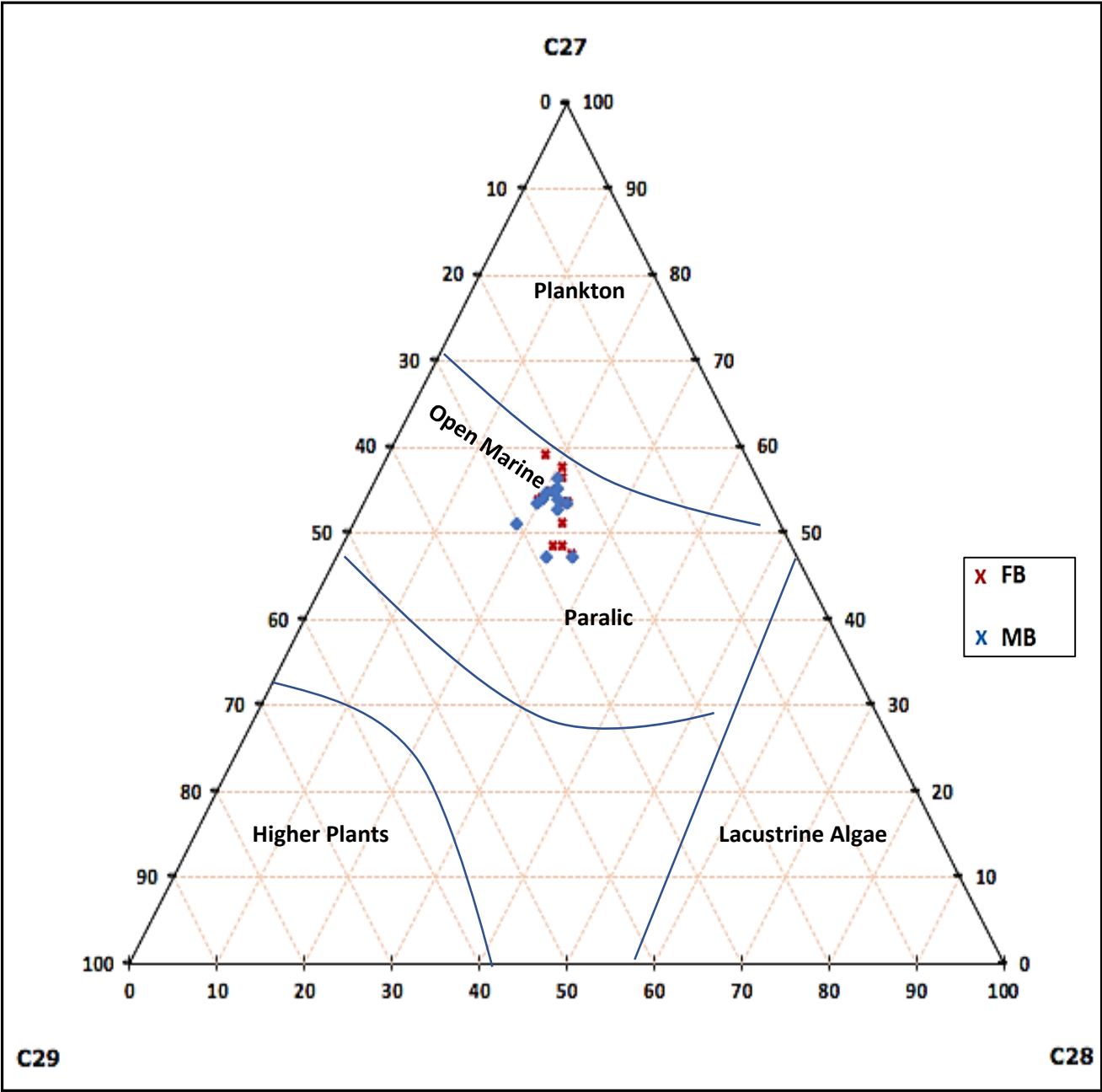


Figure 11

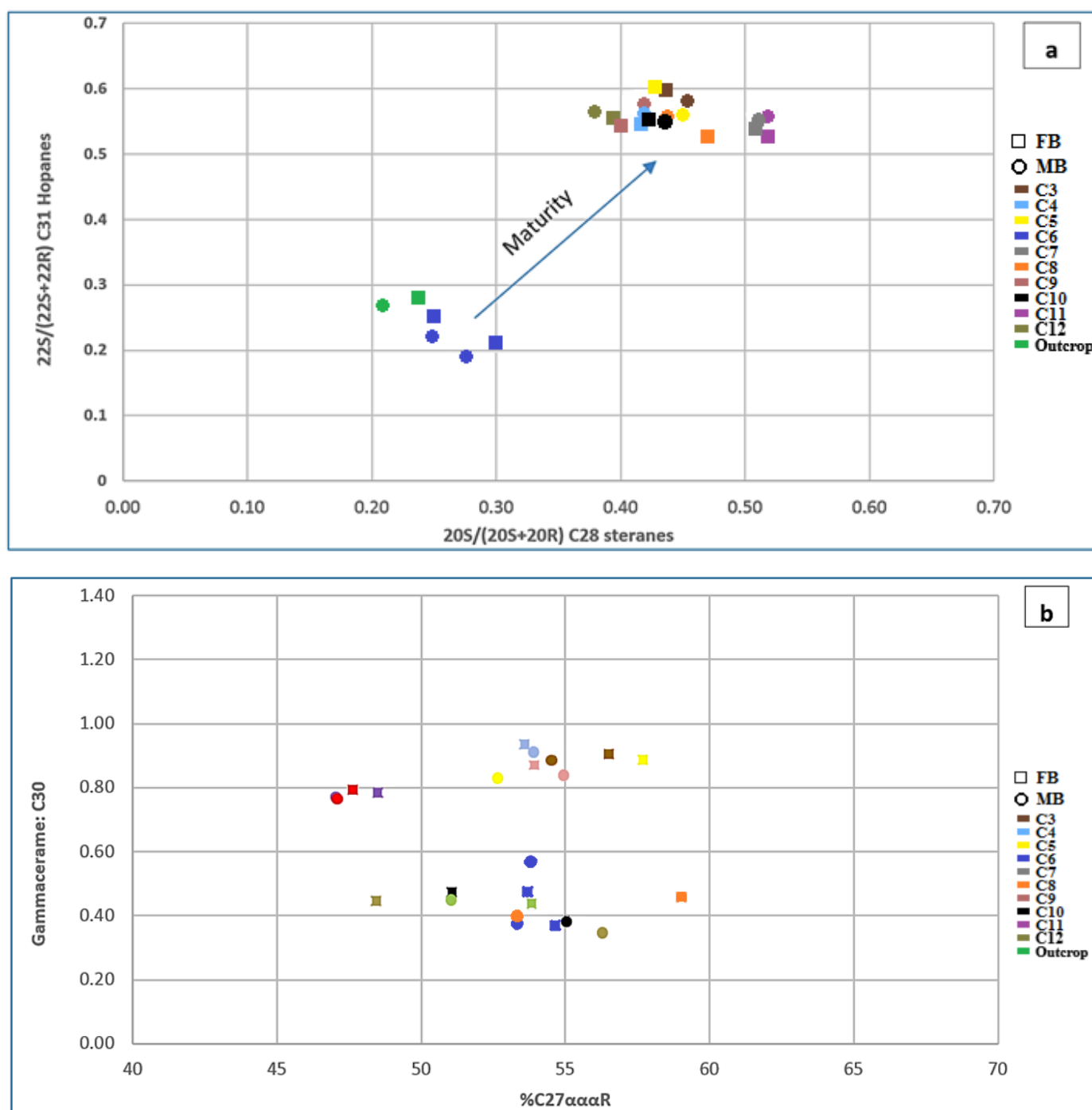


Figure 12

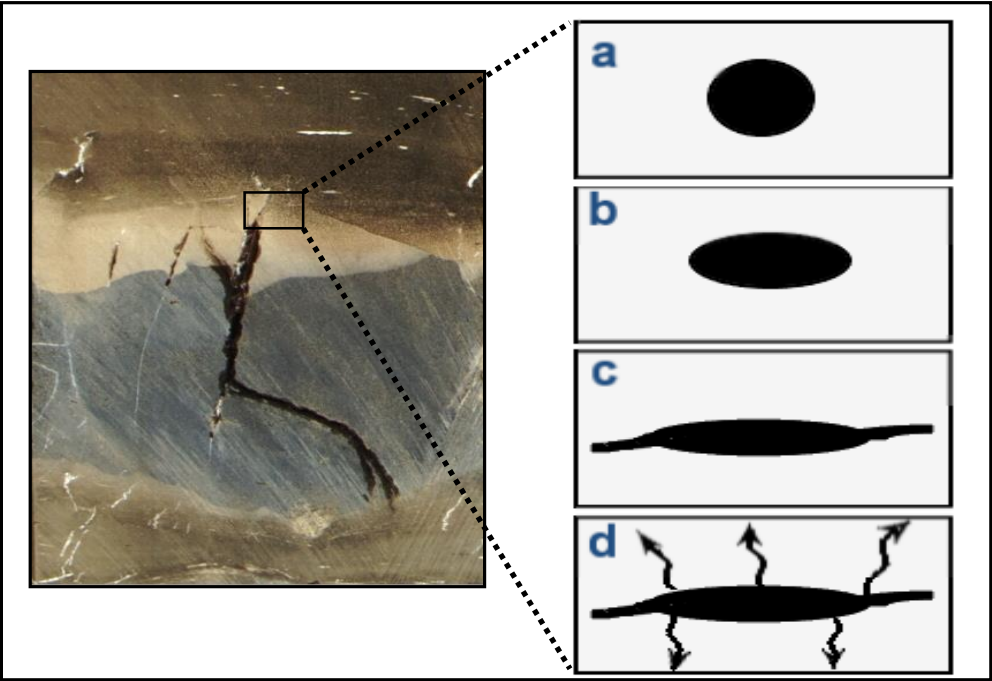
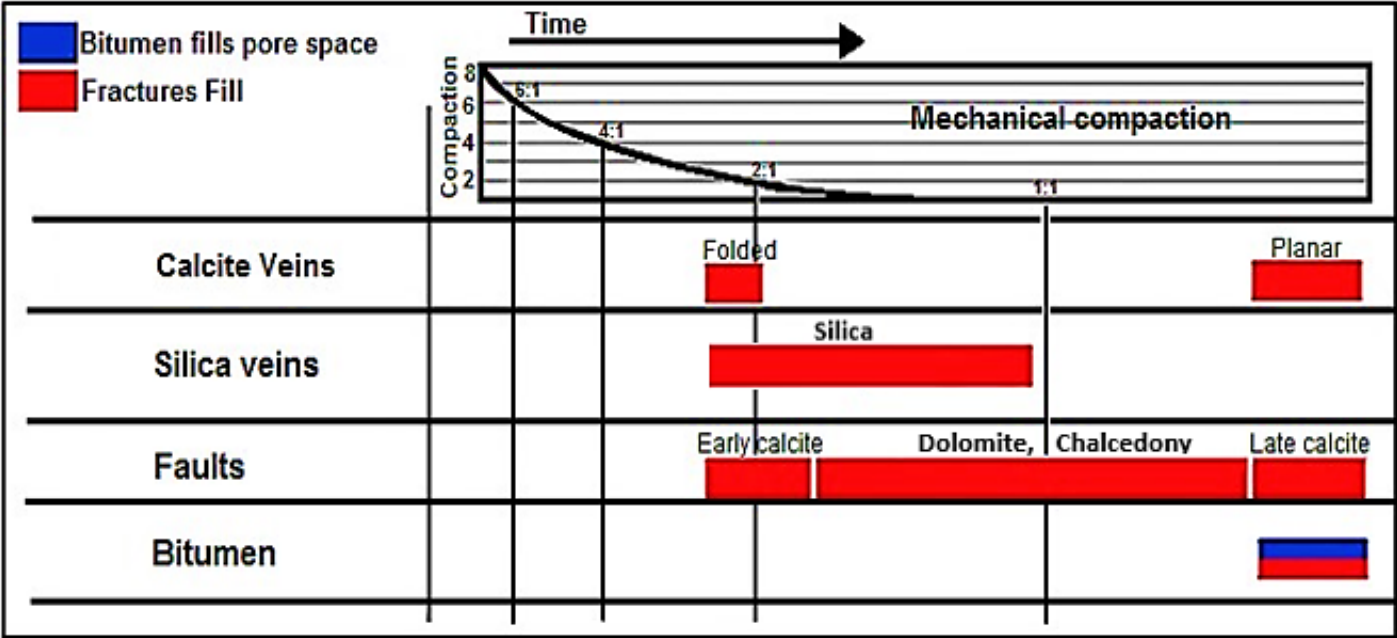


Figure 13





Click here to access/download
supplementary material (not datasets)
Supplementary data.docx

